Check for updates

ADVANCED ENERGY MATERIALS
www.advenergymat.de

Toward Low-Temperature Zinc-Ion Batteries: Strategy, Progress, and Prospect in Vanadium-Based Cathodes

Lujie Jia, Hongfei Hu, Xiaomin Cheng, Hao Dong, Huihua Li, Yongzheng Zhang, Huang Zhang, Xinyu Zhao, Canhuang Li, Jing Zhang,* Hongzhen Lin,* and Jian Wang**

Low-temperature vanadium-based zinc ion batteries (LT-VZIBs) have attracted much attention in recent years due to their excellent theoretical specific capacities, low cost, and electrochemical structural stability. However, low working temperature surrounding often results in retarded ion transport not only in the frozen aqueous electrolyte, but also at/across the cathode/electrolyte interface and inside cathode interior, significantly limiting the performance of LT-VZIBs for practical applications. In this review, a variety of strategies to solve these issues, mainly including cathode interface/bulk structure engineering and electrolyte optimizations, are categorially discussed and systematically summarized from the design principles to in-depth characterizations and mechanisms. In the end, several issues about future research directions and advancements in characterization tools are prospected, aiming to facilitate the scientific and commercial development of LT-VZIBs.

1. Introduction

Along with the popularization of new energy storage systems, the increasing demands for higher safety in turns put forward a more urgent demand for developing high-energy-density batteries, especially under low-temperature environmental conditions.[1] Thanks to the high theoretical specific capacity, the potentially low cost, and excellent safety of metallic zinc anode, aqueous zinc ion batteries (ZIBs) have become one of the main candidates for next-generation high-energy-density storage batteries.[2] Be exposed from room to low temperature condition, it demonstrates deteriorated and

L. Jia, H. Hu, X. Cheng, H. Dong, X. Zhao, H. Lin, J. Wang
i-Lab & CAS Key Laboratory of Nanophotonic Materials and Devices
Suzhou Institute of Nano-Tech and Nano-Bionics
Chinese Academy of Sciences
Suzhou 215123, China
E-mail: hzlin2010@sinano.ac.cn; wangjian2014@sinano.ac.cn; jian.wang@kit.edu

H. Li, H. Zhang
Key Laboratory of Engineering Dielectric and Applications (Ministry of Education)
School of Electrical and Electronic Engineering
Harbin University of Science and Technology
Harbin 150080, China

Y. Zhang
State Key Laboratory of Chemical Engineering
East China University of Science and Technology
Shanghai 200237, China
E-mail: zhangyongzheng@ecust.edu.cn

C. Li
Catalonia Institute for Energy Research-IREC
Department of Chemistry
University of Barcelona
Barcelona 08028, Spain

J. Zhang
School of Materials Science and Engineering
Xi'an University of Technology
Xi'an 710048, China
E-mail: zhangjing2020@xaut.edu.cn

J. Wang
Helmholtz Institute Ulm (HIU)
D89081 Ulm, Germany

J. Wang
Karlsruhe Institute of Technology (KIT)
D76021 Karlsruhe, Germany

The ORCID identification number(s) for the author(s) of this article can be found under https://doi.org/10.1002/aenm.202304010

© 2023 The Authors. Advanced Energy Materials published by Wiley-VCH GmbH. This is an open access article under the terms of the Creative Commons Attribution License, which permits use, distribution and reproduction in any medium, provided the original work is properly cited.

DOI: 10.1002/aenm.202304010

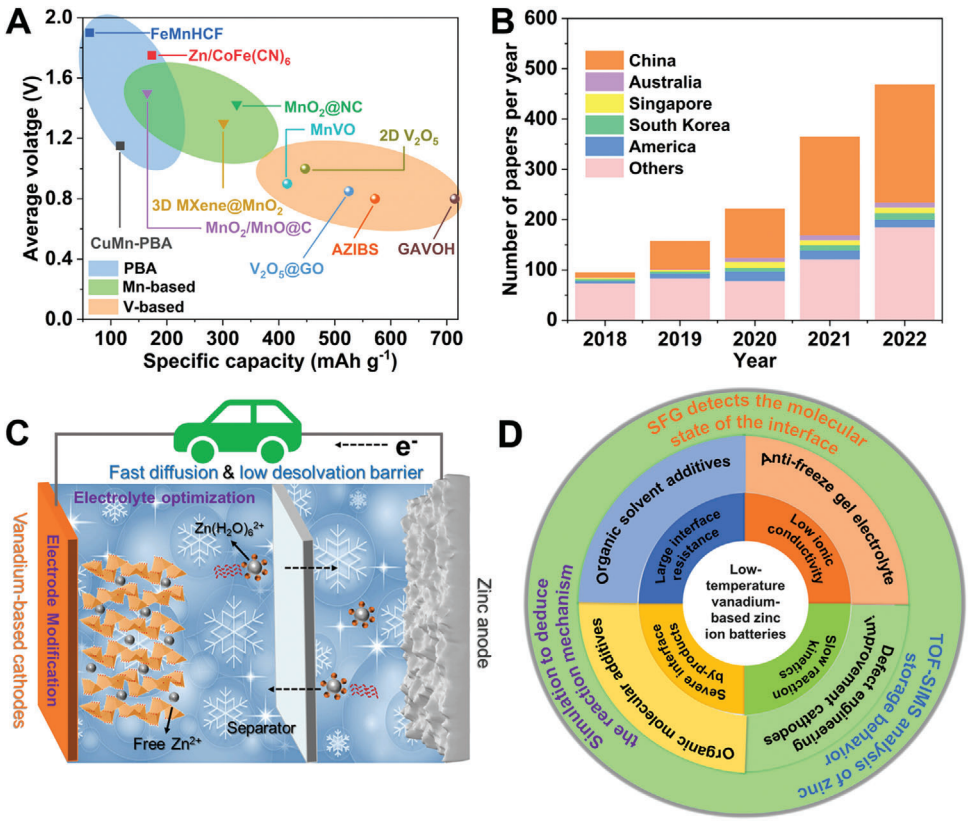

Figure 1. A) The comparison in the specific capacity and plateau voltage of different cathodes for Zn ion batteries; B) The investigation trend of the vanadium-based cathodes in Zn ion batteries in recent 5 years around the worldwide; C) Charge/discharge evolution of a low-temperature vanadium-based Zn ion battery; D) Summary of the recent foucs on the optimization strategies to low-temperature vanadium-based Zn ion batteries.

dissatisfactory electrochemical performances of ZIBs. Usually, in low-temperature operation conditions, the large solvation/desolvation energy barrier of $[Zn(H_2O)_6]^{2+}$ at the electrode/electrolyte interface is too crucial to dissociate for free isolated Zn^{2+}, if not more important than electrolyte solidification, leading to unsatisfied performances.[1d,2e,3]

For the cathodes of vanadium-based compounds (V_2O_5, $Li_xV_2O_5$, V_2O_3, MgV_2O_4, etc.),[4] manganese-based compounds (MnO_2, $ZnMn_2O_4$, etc.)[5] and Prussian blue and their analogues (PBA),[6] all exhibit remarkable Zn ion storage performance. Compared to other cathode materials, vanadium-based cathode materials tend to have better low-temperature performance and theoretical specific capacity (589 mAh g^{-1}) with moderate voltage plateau (**Figure 1**A), providing a critical option for improving the energy density of zinc ion batteries with long lifespan.[7] Apart from this, vanadium-based cathode materials also exhibit layered structure, affording the feasibility of storing Zn^{2+} and intrinsically propelling rapid Zn^{2+} diffusion.[8] In this regard, many works have pointed out that vanadium-based cathode materials are robust in realizing high-rate charging/discharging ability as high as 40 A g^{-1}.[9] Moreover, facile modification of introducing metal ions, atoms, or even molecules inside the cathode helps to expand the interlayer spacing or fabricating catalytic sites, thereby improving its diffusion kinetics under low-temperature performance.[2d]

In spite of electrolyte modification to reduce freezing point, the diffusion kinetics of Zn^{2+} in cathode via design and interface engineering strategies are attracting more and more attentions.[1d,10] However, vanadium-based ZIBs also encounter several challenging issues. For example, even though the bare radius of Zn^{2+} (0.74 Å) is very similar to that of Li^+ (0.76 Å), the larger solvation structure shell of $[Zn(H_2O)_6]^{2+}$ ($[Zn(H_2O)_6]^{2+} \rightarrow 6H_2O+Zn^{2+}$) inevitably leads to sluggish Zn^{2+} diffusion and poor interfacial charge transfer kinetics at the interface owing to the higher bivalent state and the spatial steric effect.[11] Meanwhile, the stability of vanadium-based ZIB with low current density at low temperature is also a great challenge due to the structural disintegration at high levels of cation embedding and the dissolution of vanadium in the weakly acidic electrolytes,[12] which is a spontaneous reaction as the strongly polarized water molecules corrode the crystal structure of vanadium-based cathode. This problem not only leads to capacity degradation, but also negatively affects the cyclic stability of the battery as dissolved metal ions are deposited on the electrodes causing passivation during the electrochemical process,[13] which will be more pronounced when operated at low temperatures. Under the low temperature, the behaviors of hydrate Zn^{2+} seems to be a disaster and rate-determining step owing to the limited kinetics and huge desolvation barriers, which should be further demonstrated and made clear. In addition, the zinc dendrite growth also seriously hamper the reversibility of Zn anode.[10a,14]

© 2023 The Authors. Advanced Energy Materials published by Wiley-VCH GmbH

16146840, 0, Downloaded from https://onlinelibrary.wiley.com/doi/10.1002/aenm.202304010 by Karlsruher Institut F., Wiley Online Library on [15/01/2024]. See the Terms and Conditions (https://onlinelibrary.wiley.com/terms-and-conditions) on Wiley Online Library for rules of use; OA articles are governed by the applicable Creative Commons License

Lastly, the deterioration of wettability and the generation of active water molecules at electrolyte/cathode interfaces would cause the formation of hydrogen evolution reaction.[15]

Up to date, intensive researches have been performed to solve these problems of LT-VZIBs from the aspects of cathode structure modification designs to electrolyte engineering.[16] Increasing efforts come out for achieving high-performance vanadium-based ZIBs in addressing the above issues partially around the world as summarized in Figure 1B.[3a] As discussed above, bringing the ZIBs from room-temperature to low-temperature operating environment would induce more tough and complex challenges (Figure 1C).[17] For example, when the solvated $[Zn(H_2O)_6]^{2+}$ with large solvent sheath moves to the electrode/electrolyte interface, they have to overcome the huge desolvation energy barrier before participating across the interface, which is the rate-limiting step for LT-VZIBs.[10c,18] Meanwhile, in the solid electrode interior phase, the steric hindrance effect caused by the repulsion of the lattice atoms against solvent molecules makes it extremely difficult for solvated $[Zn(H_2O)_6]^{2+}$ to diffuse at low temperature.[19] To this end, to improve the performances of LT-VZIBs is initial to reduce the desolvation energy barrier at the electrode/electrolyte interface and decrease freezing point without sacrificing ion conductivity. Although larger numbers of reviews on vanadium-based cathode or low-temperature zinc-based batteries have appeared, the discussions and analyses mainly focus on the principles of electrolyte modulations or solvation shell structure regulations for realizing low-temperature freezing point.[20] However, the sluggish Zn^{2+} diffusion kinetics are responsible for the depressive electrochemical performance. Up to date, there lacks of a comprehensive and systematic summary with respect to the local electronic effect of the cathode materials and diffusion behaviors for propelling Zn^{2+} diffusion at the interface or in the electrode interior.

In terms of recent progresses in cathode and electrolyte, the optimal strategies toward high-performance LT-VZIBs are summarized in Figure 1D. First, the cathode construction engineering strategies of vanadium-based cathodes, including metal ion doping and enrichment of anion/cation vacancies are reviewed from the perspective of electron density, aiming at enhancing the structural stability, improving the ionic conductivity or expanding layer spacing to provide pathways for free Zn^{2+} transport. Second, electrolyte optimization strategies for regulating solvation shell such as high-concentration electrolytes, electrolyte additives, and gel electrolytes are summarized, decreasing the freezing point of electrolyte, passivate interfacial water molecules, and reducing the desolvation energy barrier. Thirdly, the application of advanced characterization tools for in-depth investigation and mechanism of LT-VZIBs are briefly reviewed and prospected

2. Cathode Structure Engineering for Fast Zn^{2+} Desolvation and Diffusion

As well known, the physicochemical properties of cathode materials are the decisive factors for insertion/extraction, which determines the performances of battery systems.[1c] As discussed above, in the low-temperature surroundings, the ideal cathode materials should reach the following demands:[2d,3a,15c,21] 1) rapid electronic conductivity within cathode networks; 2) fast dissociation kinetics from $[Zn(H_2O)_6]^{2+}$ to generate bare free Zn^{2+} at the interface; 3) fast ion diffusion kinetics in the cathode interior to reach the maximum capacity; 4) robust cathode/electrolyte interphase formation with rapid Zn exchange. For the cathode, the metal ion in cathode also dissolute in the electrolyte when charging/discharging, deteriorating the crystal structure. From the viewpoint of electronic density, the dissolution of V can be also interpreted by the electronic density redistribution. Generally, doping effects via metallic cations such as Mg, Ca, Na, and non-metallic anions like O, N, P, S, etc., are capable of redistributing the local electronic density with high electronic conductivity and fast ion diffusion kinetics, inhibiting the structure destroy after insertion/extraction.[2a,d,22] Another strategy is defect engineering on the cathodes, including surface and bulk defects, becoming an effective method to redistribute electronic density and improve the activity sites at the interface.[23] In this section, the electronic density modifications via metallic cation doping, non-metallic anion doping, and defect construction are briefly introduced.

2.1. Metal Cation Doped Vanadium-Based Cathodes

Extensive investigations have revealed that the doping of metal cations and cationic groups into vanadium-based materials can greatly improve the ion diffusion kinetics and enhance the intrinsic electronic conductivity of cathodes due to the increased interlayer spacing. The dopants reinforce their structural stability with robust electronic density distribution during cycling.[24] With in-depth research, various types of dopant ions ranging from the main group metal ions with weak electronegativity such as K^+, and Mg^{2+} etc., to the transition metal ions with tunable *d*-orbital electronic structures such as Mn^{2+}, and Cu^{2+} etc. have revealed and shown their vital functions in improving the Zn^{2+} storage capacity and cycling stability.[2d,25]

In general, weakly electronegative main group ions doped into vanadium-based materials can be tightly bound to the vanadium-based internal crystal structures such as square cones and trigonal cones to ensure fast diffusion kinetics and improve their structural stability.[26] For layered vanadium-based oxides, the limited 2D ion diffusion path makes the reaction rate extremely slow. It was designed that K^+ was doped into the interlayer of V_2O_5 along the b-direction (**Figure 2A**), forming the pure monoclinic crystalline of $K_{0.5}V_2O_5$ (KVO) (Figure 2B).[25a] In this manner, a wider layer spaced KVO is generated and delivers an ideal Zn ion diffusion coefficient from 10^{-12} to 10^{-11} cm^2 s^{-1} (Figure 2C). Assembling in full Zn//KVO cells tested at a low temperature of −20°C, an ultrahigh discharge capacity of 317 mAh g^{-1} was displayed at a current density of 0.1 A g^{-1}, demonstrating superior low-temperature diffusion kinetics. Similarly, a discharge capacity of 241 mAh g^{-1} delivered after 1000 cycles at 1 A g^{-1}, showing an excellent structural stability at low temperatures.

Not coincidentally, to further advance the industrial application of LT-VZIBs, a larger radius of Mg^{2+} is introduced into V_2O_5 crystal to form $Mg_{0.19}V_2O_5{\cdot}0.99H_2O$ (δ-MgVO) electrode with an extra-large layer spacing of ≈13.4 Å (Figure 2D), which greatly improved the solvated ion diffusion kinetics inside the cathode at low temperatures. In conjunction with an anti-freeze gel electrolyte (Figure 2E).[25b] Increasing the cathode loading to

© 2023 The Authors. Advanced Energy Materials published by Wiley-VCH GmbH

16146840, 0, Downloaded from https://onlinelibrary.wiley.com/doi/10.1002/aenm.202304010 by Karlsruher Institut F., Wiley Online Library on [15/01/2024]. See the Terms and Conditions (https://onlinelibrary.wiley.com/terms-and-conditions) on Wiley Online Library for rules of use; OA articles are governed by the applicable Creative Commons License

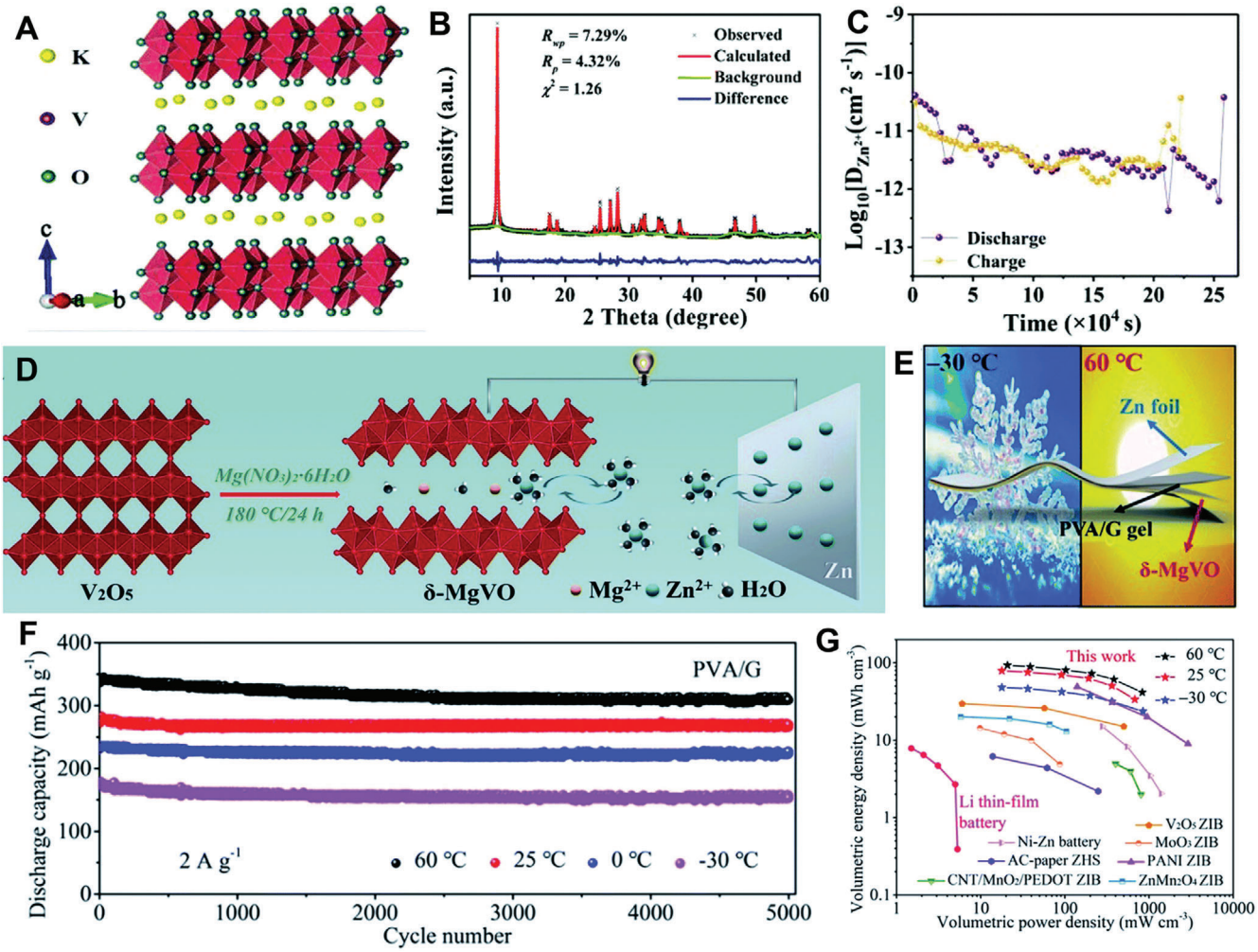

Figure 2. A) Crystalline illustration of K^+ doping into the V_2O_5. B) The XRD pattern of KVO. (C) The Zn^{2+} diffusion coefficient of the KVO cathode. Reproduced with permission.[25a] Copyright 2021, The Royal Society of Chemistry. D) Schematic diagram showing the formation process of δ-MgVO and the working principle of the Zn//δ-MgVO battery. E) The schematic diagram of thin-film PVA/G Zn//δ-MgVO battery. F) Cycling performance at 2.0 A g^{-1} under different temperatures. G) Volumetric Ragone plots in comparison with those of previously reported energy storage devices (these devices in other reports were all measured at room temperature). Reproduced with permission.[25b] Copyright 2021, The Royal Society of Chemistry.

commercial levels as high as 10 mg cm^{-2}, the assembled Zn//δ-MgVO full cells exhibited an astonishing cycling stability verified from 60 to -30 °C. After 5000 cycles, robust capacities of ≈309, 270, 227, and 153 mAh g^{-1} were maintained at 60, 25, 0, and -30 °C, respectively, with the capacity retention rates of 91.7%, 99.0%, 98.2%, and 87.7%, respectively (Figure 2F). Moreover, the volumetric energy density exhibited by the full cell was much more advantageous even compared to other batteries under ambient temperatures at that time (Figure 2G).

In the case of transition metal ions with tunable *d*-orbital electronic structures, the interlayer doping is essentially similar to the main group ions. However, the difference is that the main purpose of transition metal ions doping is to improve the electrical conductivity of cathode, regulate the intrinsic electronic density distribution, and promote electrochemical behaviors.[26–27] In reality, the application of adjustable *d*-orbital electrons can help the system to achieve more functions.[1h,28] For example, the unfilled *3d* orbitals with more shared electron orbitals promote more electron transfer, reduce the impedance, and accelerate the reaction kinetics inside the electrode. Cao et al. had designed the introduction of Mn^{2+} in vanadium-based oxide, which had a certain catalytic effect and simultaneously promoted the electron transfer, resulting in a significant improvement in electrochemical performance.[26,29] In addition, unlike the main group ions, the dopant of transition metal Mn^{2+} brought about a reduction in the original layer spacing from 14.39 to 13.26 Å (**Figure** 3A). Due to the tight binding energy between the doped Mn^{2+} and the negatively charged VO_6 units, the charge transfer resistances were decreased along with the increase of cycles, contributing to the enhanced structural stability, and facilitated ion transport (Figure 3B). Meanwhile, the superior zinc ions diffusion coefficient was achieved, i.e., 10^{-12} to 10^{-10} cm^2 s^{-1} (Figure 3C). With the introduction of Mn^{2+} into crystal host material, the calculation shows that interlayer charge state of V_2O_5 was altered and a new energy level appeared near the Fermi level (Figure 3D). Therefore, the band gap was reduced to ≈40% of that in the

© 2023 The Authors. Advanced Energy Materials published by Wiley-VCH GmbH

16146840, 0, Downloaded from https://onlinelibrary.wiley.com/doi/10.1002/aenm.202304010 by Karlsruher Institut F., Wiley Online Library on [15/01/2024]. See the Terms and Conditions (https://onlinelibrary.wiley.com/terms-and-conditions) on Wiley Online Library for rules of use; OA articles are governed by the applicable Creative Commons License

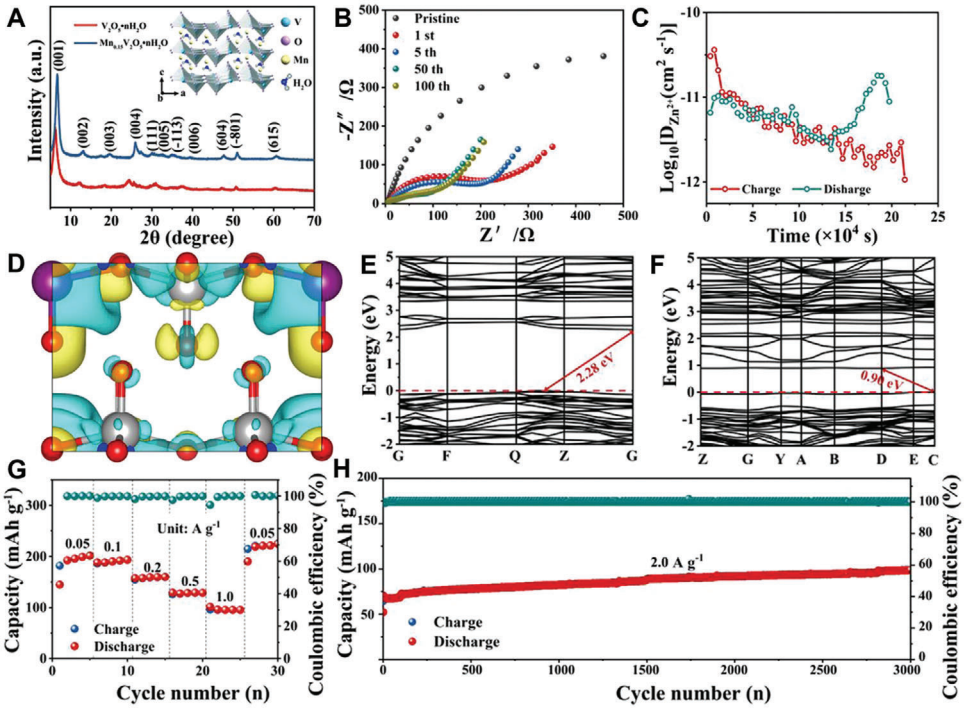

Figure 3. A) The XRD patterns of $Mn_{0.15}V_2O_5{\cdot}nH_2O$ and $V_2O_5{\cdot}nH_2O$. B) Nyquist plots of $Mn_{0.15}V_2O_5{\cdot}nH_2O$ cathode before and after cycling at room temperature. C) The Zn^{2+} diffusion coefficient of the $Mn_{0.15}V_2O_5{\cdot}nH_2O$ cathode. D) Electron density difference of Mn^{2+}-doped V_2O_5, charge accumulation is in yellow and depletion in blue. Calculated total band structures for E) pure V_2O_5 and F) Mn^{2+}-doped V_2O_5. G) Rate capacities at various current densities at -20 °C. H) Long cycling performance at 2.0 A g^{-1}. Reproduced with permission.[2d] Copyright 2019, WILEY-VCH.

original V_2O_5 from 2.28 to 0.9 eV, implying a considerable improvement in its electrical conductivity (Figure 3E,F). In addition, the interaction and charge redistribution between vanadium and manganese ions in different valence states result in a series of changes in the concentration of ionic and electronic defects in the host material, accelerating the diffusion of zinc ions and improving the electron transfer kinetics. At an ambient temperature as low as −20°C, the battery still displayed a high-rate performance with the current densities increasing from 0.05 to 1.0 A g^{-1}, achieving discharge capacities of 202 and 96 mAh g^{-1}, respectively. Switching the current density back to 0.05 A g^{-1}, the capacity returns to its initial value, displaying the robustness (Figure 3G). Even at a high current density of 2.0 A g^{-1}, a high specific capacity of 100 mAh g^{-1} could be maintained over 3000 cycles (Figure 3H).[2d] Despite great progress achieved in metal cation doping, in-depth understanding of current researches on LT-VZIBs is still absent and the concise tools monitor expanding the layer spacing should be developed.

2.2. Non-Metallic Anion Doped Vanadium-Based Cathodes

For vanadium-based composites, although cation doping is an effective approach to regulate the electronic density by adjusting crystal structures, these extra metal ions with higher atomic weight would sacrifice the storage of Zn^{2+} and decrease the entire energy density, causing lower theoretical specific capacity.[30] Instead of cation, anion doping such as S, F, P, N, etc. is considered to be an alternative to increase the electronic conductivity without increasing too much weight.[22a] For the most common metal oxide cathodes, the process of zinc ions insertion can be difficult due to the strong electronegativity of oxygen, yet the use of heterogeneous atomic doping with weak electronegativity can effectively attenuate the electrostatic interactions.[31]

Since there exists a lone electron pair in nitrogen atom, acting as a carrier to promote the electron redistribution, N doping strategy can effectively avoid the atom agglomeration.[32] For example, the creation of a nitrogen-doped vanadium dioxide/nitrogen-doped carbon (N-VO_2@NC) heterostructure was designed with abundant active sites via the thermal decomposition of vanadium oxide (VO_x)/polypyrrole (PPy) on carbon nanotube fibers (CNTF) (**Figure 4**A), significantly improving the activity of the electrode material.[30c] Moreover, the theoretical calculation results indicated that the band gap of PPy-assisted generated N-VO_2 was reduced from 0.55 to 0.23 eV (Figure 4B), which facilitated the excitation of charge carriers to the conduction band, contributing to a significant enhancement of the electronic conductivity of the composite. In addition to single anion doping, experiments have confirmed N-doped vanadium oxide will also bring about a large number of oxygen defects during the doping process, which further facilitates ions diffusion and electron conduction by lowering the diffusion energy barrier of zinc ions.[33]

Compared with F and N doping, S atom shows the largest atomic radius and the lowest electronegativity, which can greatly expand the layer spacing, reduce the energy barrier for Zn^{2+} diffusion, and promote its diffusion kinetics.[34] By replacing some of the oxygen atoms in vanadium oxides with S atoms through sulfidation reaction, abundant oxygen defects are created to

© 2023 The Authors. Advanced Energy Materials published by Wiley-VCH GmbH

16146840, 0, Downloaded from https://onlinelibrary.wiley.com/doi/10.1002/aenm.202304010 by Karlsruher Institut F., Wiley Online Library on [15/01/2024]. See the Terms and Conditions (https://onlinelibrary.wiley.com/terms-and-conditions) on Wiley Online Library for rules of use; OA articles are governed by the applicable Creative Commons License

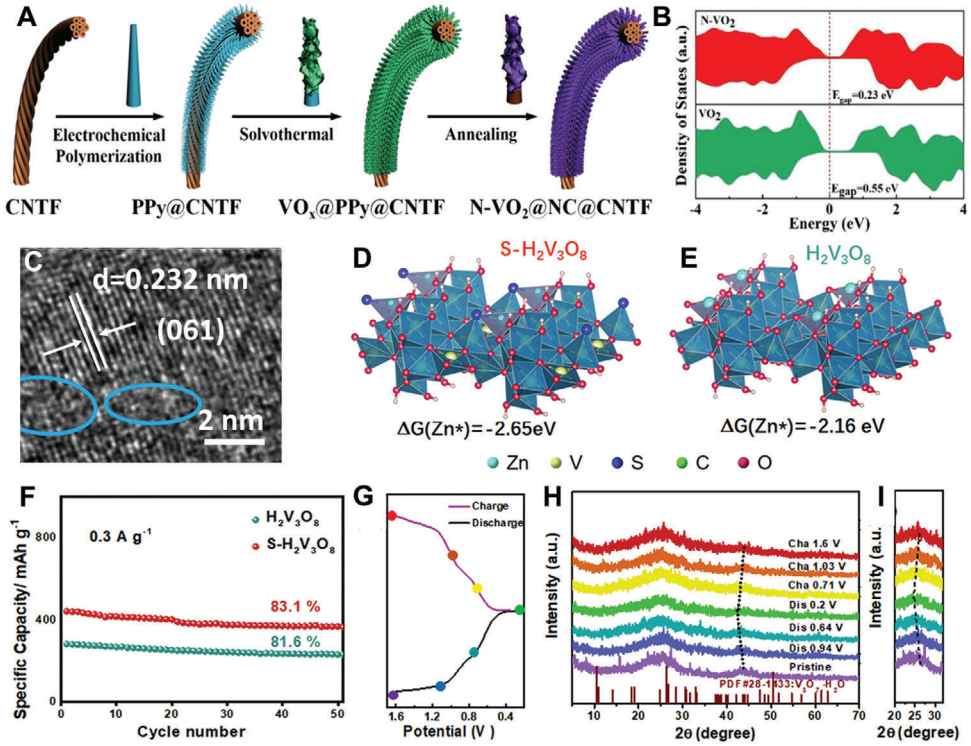

Figure 4. A) Schematic illustration of preparation of N-VO_2@NC@CNTF B) The corresponding density of states of VO_2 and N-VO_2. Reproduced with permission.[30c] Copyright 2022, WILEY-VCH. C) TEM images of S-$H_2V_3O_8$ nanofibers. The adsorb free energy of D) S-$H_2V_3O_8$ and E) $H_2V_3O_8$. F) Cycling performance at 0.3 A g^{-1}. G) GCD curve and corresponding H) and I) ex-situ XRD patterns at different states. Reproduced with permission.[30d] Copyright 2022, Elsevier.

obtain the S-$H_2V_3O_8$ cathode as well (Figure 4C). With the assistance of theoretical calculations, S-$H_2V_3O_8$ cathode possessed a lower band gap and a higher Zn^{2+} adsorption energy compared to $H_2V_3O_8$ from −2.16 to 2.65 eV (Figure 4D,E), which enhanced the charge transfer rate at the interface and improved the zinc ions diffusion kinetics.[30d] With the expanded layer spacing and increased active sites (Figure 4C), the resulted S-$H_2V_3O_8$ cathode showed a cyclic stability with a capacity retention of 83.1% and Coulombic efficiency of almost 100% after 50 cycles at 0.3 A g^{-1} in comparison to that of $H_2V_3O_8$ (81.6%) (Figure 4F). Furthermore, the ex-situ XRD was employed to investigate the charge storage process and the electrochemical reaction mechanism of the S-$H_2V_3O_8$. As shown in Figure 4G–I, in the first fully charge/discharge cycle at 0.3 A g^{-1}, the peaks at 26.4° and 43.9° attributing to the crystal face of (101) and (341) gradually shift to a lower degree in the discharging process and then move positively to the original degree during the charging process, which represents interlayer distance increases firstly and then decreases coming from the excellent reversibility of Zn^{2+} de-/intercalation. Since most of the anion doping has been studied at room temperature so far, only an outlook on its application prospects at low temperatures will follow.

Currently, the researches on LT-VZIBs have mainly focused on cation doping to improve the electron conductivity of cathode material or accelerate the ion diffusion kinetics inside the cathode to enhance the battery performance. Remarkably, anion doping has a similar function of cation but is also rarely reported at low temperature, and the absence of specific case studies does not mean that it is not meaningful.[35] These weaker electronegative anions are deemed to play an essential role in promoting the insertion/extraction behaviors of Zn ions in LT-VZIBs, which needs to be further studied and understood in depth. Other than that, there is also a little-known but critical issue of facilitating the desolvation reaction at the cathode/electrolyte interface under low temperatures to obtain highly reactive free zinc ions, which is extremely critical to achieve high energy density LT-VZIBs.[1d,36] In fact, both the carrier exchange within cathode networks and the dissociation kinetics from $[Zn(H_2O)_6]^{2+}$ to generate free Zn^{2+} at the interface are degenerated as the surrounding temperature decreased to below 0 °C. On the other hand, the inflated larger solvation structure shell with bigger hydrate radius at low temperature may significantly induce the accessible insertion of $[Zn(H_2O)_6]^{2+}$ into the layers of the vanadium-based compounds, greatly decreasing the ion diffusion kinetics in the cathode interior and/or at the cathode/electrolyte interface. Apart from improving the intrinsic electronic conductivity, the anion doping is also quite potential to change the local current density of the vanadium-based compounds, forming active sites to reduce the energy barrier for Zn^{2+} diffusion and promote its diffusion kinetics for many Zn^{2+} storage. In the future, the strategy of anion doping for high-performance LT-VZIBs should pay more attention to strengthen the desolvation capability at the cathode/electrolyte interface to release more free zinc ions and further broaden the layer spacing of the vanadium-based compounds to fasten ion diffusion kinetics at the premise of improved intrinsic electronic conductivity of the cathodes.

© 2023 The Authors. Advanced Energy Materials published by Wiley-VCH GmbH

16146840, 0, Downloaded from https://onlinelibrary.wiley.com/doi/10.1002/aenm.202304010 by Karlsruher Institut F., Wiley Online Library on [15/01/2024]. See the Terms and Conditions (https://onlinelibrary.wiley.com/terms-and-conditions) on Wiley Online Library for rules of use; OA articles are governed by the applicable Creative Commons License

2.3. Intrinsic Defects Engineering for Vanadium-Based Cathodes

Since most of the electrochemical reactions occur at the electrode/electrolyte interface, surface defects of cathode materials would make the interface more active than bulks and become research focus.[3b,23b,c,37] Usually, the defects are generally divided into extrinsic defects and intrinsic defects.[34b] Extrinsic defects such as anions/cations doping defects, consist of impurity atoms or impurity ions embedded in the lattice, while intrinsic defects such as anion/cation vacancies defects are formed by the deviation or removal of crystal itself from the lattice structure, e.g. thermal motion of atoms or ions at lattice junctions without changing the overall crystal composition.[38] Unlike extrinsic defects induced by doping effect, vacancy produced by chemical removal and thermal reduction are intrinsic defects, which play important parts in regulating the surface properties and electronic structure of cathodes:[22d,34a,36,37c,39] (1) improving ion/electron diffusion kinetics in the cathode interior; (2) generating more interfacial active sites to improve the capability of zinc ion storage; (3) reducing the low reaction energy barriers with fast interfacial desolvation. Essentially, the introduction of vacancy defects allows the redistribution of electron density in the host materials, resulting in the establishment of a catalytically active centers,[23c] therefore, controlling defects and further comprehending the mechanisms is inevitable for LT-VZIBs. In this part, the defect engineering methods to improve the capability of Zn^{2+} desolvation and diffusion for achieving high electrochemical performance of batteries at low temperatures are summarized

As we all know, most vanadium-based materials are oxygen-containing compounds with different ratios. Abundant oxygen vacancies can be obtained through a simple partial reduction treatment without changing the surface morphology.[22a,23c] By removing oxygen atoms from the pristine V_6O_{13} (p-VO) lattice, the oxygen-deficient V_6O_{13} (O_d-VO) composites are formed on graphene oxide (**Figure 5A**), thus providing rich sites for allowing zinc ions to be rapidly inserted into the electrode interior. Moreover, the strong formed chemical bonds between Zn and O prevent the release of Zn^{2+} during charging because of the strong Coulombic ionic lattice interaction between divalent Zn^{2+} and the metal oxides (Figure 5B). As the cell cycles, these inactive Zn^{2+} gradually accumulated and formed a physical barrier on the cathode, which reduced the number of active sites for Zn^{2+} storage and hindered electron transfer of reactions inside the cathode, thus severely deteriorating the cycling stability. However, in the presence of oxygen defects, the negative oxygen atoms that interacted intensely with divalent Zn^{2+} were partially extracted from the vanadium oxide lattice (Figure 5B), thus promoting a highly reversible insertion/extraction behavior of Zn^{2+} during the cycling process. Comparing with the conventional Zn^{2+} intercalation into the ab-plane of perfect vanadium oxide, oxygen-deficient sites could open the vanadium oxide layer and allowed Zn^{2+} diffusion/intercalation along the c-axis, thus greatly promoting the reaction kinetics and electrochemical reactivity (Figure 5C,D).[2b] As a result, the galvanostatic intermittent titration technique (GITT) measurements revealed that the average Zn^{2+} diffusion coefficients in the discharged and charged states were about 1.1×10^{-11} and 0.4×10^{-11} cm^2 s^{-1}, respectively. At current densities of 0.2, 0.5, 1.0, and 2.0 A g^{-1}, the reversible specific capacities of 401, 366, 321, and 279 mAh g^{-1} were achieved, respectively. Even at a high current density of 5 A g^{-1}, an ultra-high discharge capacity of 223 mAh g^{-1} was provided.

Even if its application extends to harsh cryogenic environments, the oxygen defects also play a critical role that cannot be ignored in promoting the electrode reaction kinetics. By simulating the diffusion behaviors of free Zn^{2+} in the crystal structure, three types of oxygen-deficient sites were identified, namely, terminal site, bridge site-1, and bridge site-2 (Figure 5E).[40] The diffusion energy barriers of the anoxic sites of terminal site and bridge site-1 were 1.0 and 1.1 eV, respectively, much lower than that on perfect $NH_4V_4O_{10}$ one (2.2 eV). At the same time, the oxygen defect of bridge site-2 was generated at the bottom, away from the Zn^{2+} diffusion layer, which weakened the role of electron donor, promoted the diffusion kinetics of zinc ions, made the insertion/extraction reaction highly reversible. Thus, the same zinc ions diffusion coefficient at -30 °C was obtained as normal temperature, i.e.,$\approx10^{-9}$ cm^2 s^{-1}. Under -30 °C, the oxygen defective-rich $NH_4V_4O_{10\text{-}x}\cdot nH_2O$ (NVOH) cathode delivered specific capacities of 400, 209, and 94 mAh g^{-1} at 0.05, 1.0, and 3.0 A g^{-1}, respectively, and the reversible capacity of ≈380 mAh g^{-1} when the current density went back to 0.05 A g^{-1} (Figure 5F). Even cycled at 2 A g^{-1}, a stable Coulombic efficiency was maintained with a reversible capacity of 145.5 mAh g^{-1} after 2600 cycles (Figure 5G,H).[2a]

Currently, the majority of intrinsic defects in cathode materials cycled at low temperatures are described as a function of oxygen vacancies, while other anion defects or cation defects have never been involved.[22a] Unlike the reaction at room temperature, the decisive steps of the reaction inside the battery at low temperature are ion diffusion, electron conduction, and interfacial desolvation.[3d] Cathode/electrolyte interface, as an essential component at low-temperature, should reduce the interfacial desolvation energy barrier so that the obtained free Zn^{2+} can diffuse rapidly inside the electrode and participate in the electrochemical reaction. However, the related researches are extremely rare and this field is still an unsigned blank area.[10b] Generally, the introduction of vacancy defects could provide many catalytic sites to allow reducing the low reaction energy barriers with fast interfacial $[Zn(H_2O)_6]^{2+}$ desolvation and generating more interfacial active sites to improve zinc ion diffusion kinetics in the cathode interior together with the robust interfacial cathode/electrolyte interphase (CEI) layer formation. Considering the depressive kinetics at low temperature, higher concentration of defect in the cathodes is more favorable to improve the catalytic sites due to that the redistribution of electronic structure would bring in higher reaction kinetics in zinc ion desolvation, diffusion, and storage. However, the metal oxides with much higher defect concentration are possible to burst into the structure degradation or even collapse, which would threaten the capacity and lifespan of the LT-VZIBs. In this view, a trade-off between the high activity and the structural stability should be taken into account. Thereby, it is critical to seek the relationships between the performance and the stability of cathode structure and to gain the accurate manipulation of the defect concentration to tailor the surface electronic structure of the vanadium-based cathode for reinforced the capability of zinc ion desolvation, diffusion, and storage. In this regard, further characterization exploration, and visualization of the defects in the cathode chemistry should be a continuous pursuit for stabilizing the electrochemical performance.

© 2023 The Authors. Advanced Energy Materials published by Wiley-VCH GmbH

16146840, 0, Downloaded from https://onlinelibrary.wiley.com/doi/10.1002/aenm.202304010 by Karlsruher Institut F., Wiley Online Library on [15/01/2024]. See the Terms and Conditions (https://onlinelibrary.wiley.com/terms-and-conditions) on Wiley Online Library for rules of use; OA articles are governed by the applicable Creative Commons License

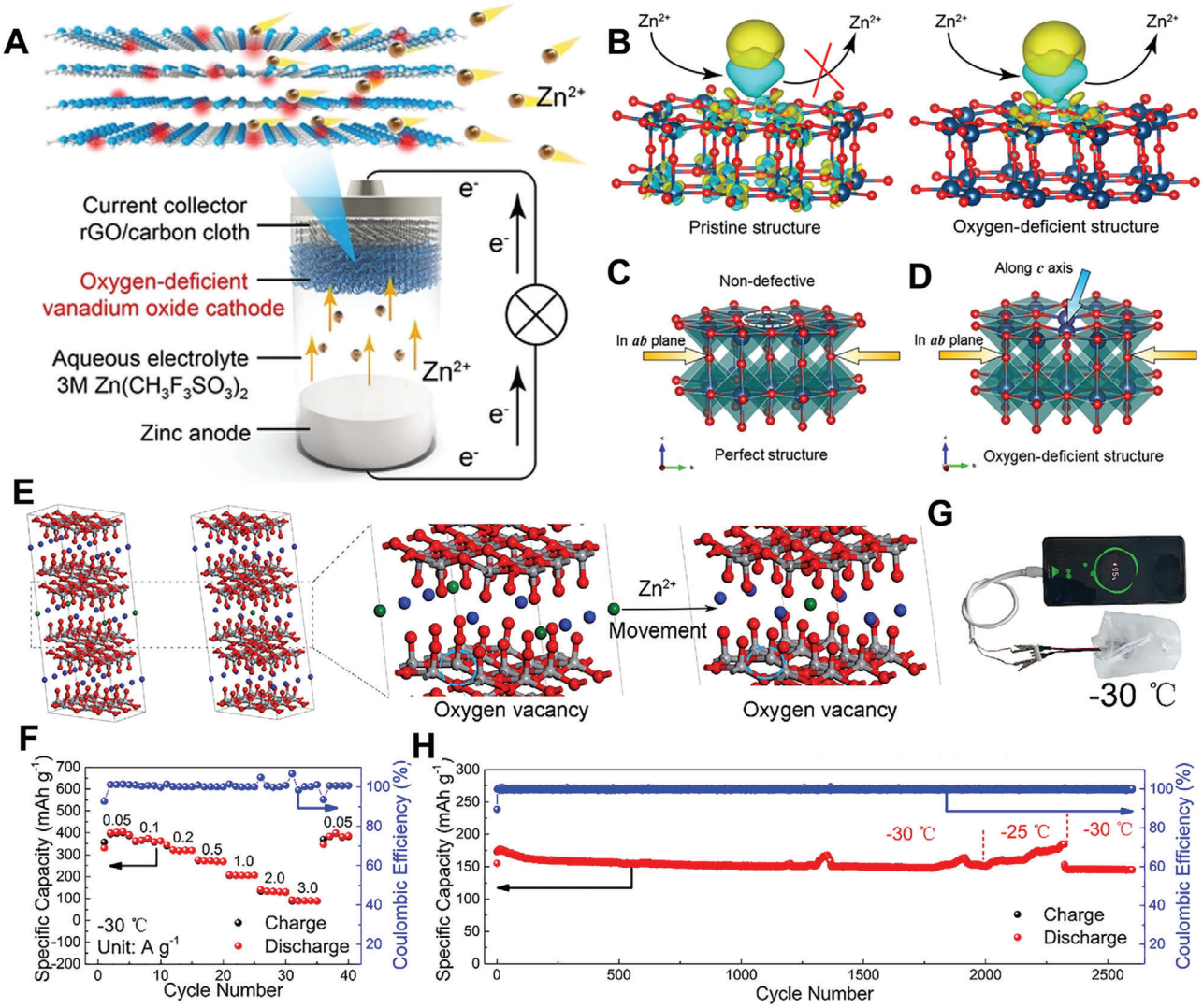

Figure 5. A) Configuration of the Zn//O_d-VO battery and the oxygen-deficient sites (represented by red spheres) are incorporated into the vanadium oxide framework. B) Illustrations of the Zn^{2+} storage/release for pristine vanadium oxide (p-VO) and oxygen-deficient vanadium oxide (O_d-VO). C) Embedding path of Zn^{2+} in the perfect structure along the ab-plane. D) Embedding path of Zn^{2+} in the oxygen-deficient structure along the ab-plane and c-axis. Reproduced with permission.[2b] Copyright 2019, WILEY-VCH. E) Schematic illustration of Zn^{2+} diffusion in NVOH with oxygen vacancy at terminal site, red balls are O atoms, blue balls are N atoms (NH^{4+} ions), green balls are Zn^{2+} ions, grey balls are V atoms. F) Rate performance of NHVOH. G) Photograph of a discharging phone powered by four cells in series in a -30 °C cryogenic box. H) Cycling performance at 2.0 A g^{-1} under different temperature. Reproduced with permission.[2a] Copyright 2020, Elsevier.

3. Aqueous Electrolyte Engineering for Cyclable LT-VZIBs

Generally, the physiochemical properties of electrolyte determines interface information, freezing point, and solvation shell structure at ambient/extreme conditions.[41] Thanks to the aqueous system, the electrolytes of ZIBs deliver unparalleled features exceeding organic electrolyte in lithium ion batteries, such as higher ionic conductivity, low cost, and environment friendliness, affording great potentials in future energy storage grid.[42] However, as research proceeded, it is found that the further advancement of ZIB has greatly been hindered by the electrolyte corrosion and side reactions of hydrogen evolution reaction when cycled under high deposition capacity.[10b,43] The application of aqueous electrolyte with water as solvents under low temperature environment inevitably encounters the following problems:[44] (1) solidification of solvent leads to huge diffusion barriers and even direct battery failure; (2) increased viscosity with cross-linked hydrogen bond causes sharp decrease in ionic conductivity; (3) severe solvation shell with higher force leads to sluggish transport and huge barrier at the electrode interface and interior.[15a] To deal with above problems, the development of electrolyte then gradually evolved into the following categories: (1) high-concentration salt electrolytes (water-in-salt); (2) organic additive electrolytes; and (3) hydrogel electrolytes. The following will detail the improvement of LT-VZIBs by optimizations measures.

© 2023 The Authors. Advanced Energy Materials published by Wiley-VCH GmbH

16146840, 0, Downloaded from https://onlinelibrary.wiley.com/doi/10.1002/aenm.202304010 by Karlsruher Institut F., Wiley Online Library on [15/01/2024]. See the Terms and Conditions (https://onlinelibrary.wiley.com/terms-and-conditions) on Wiley Online Library for rules of use; OA articles are governed by the applicable Creative Commons License

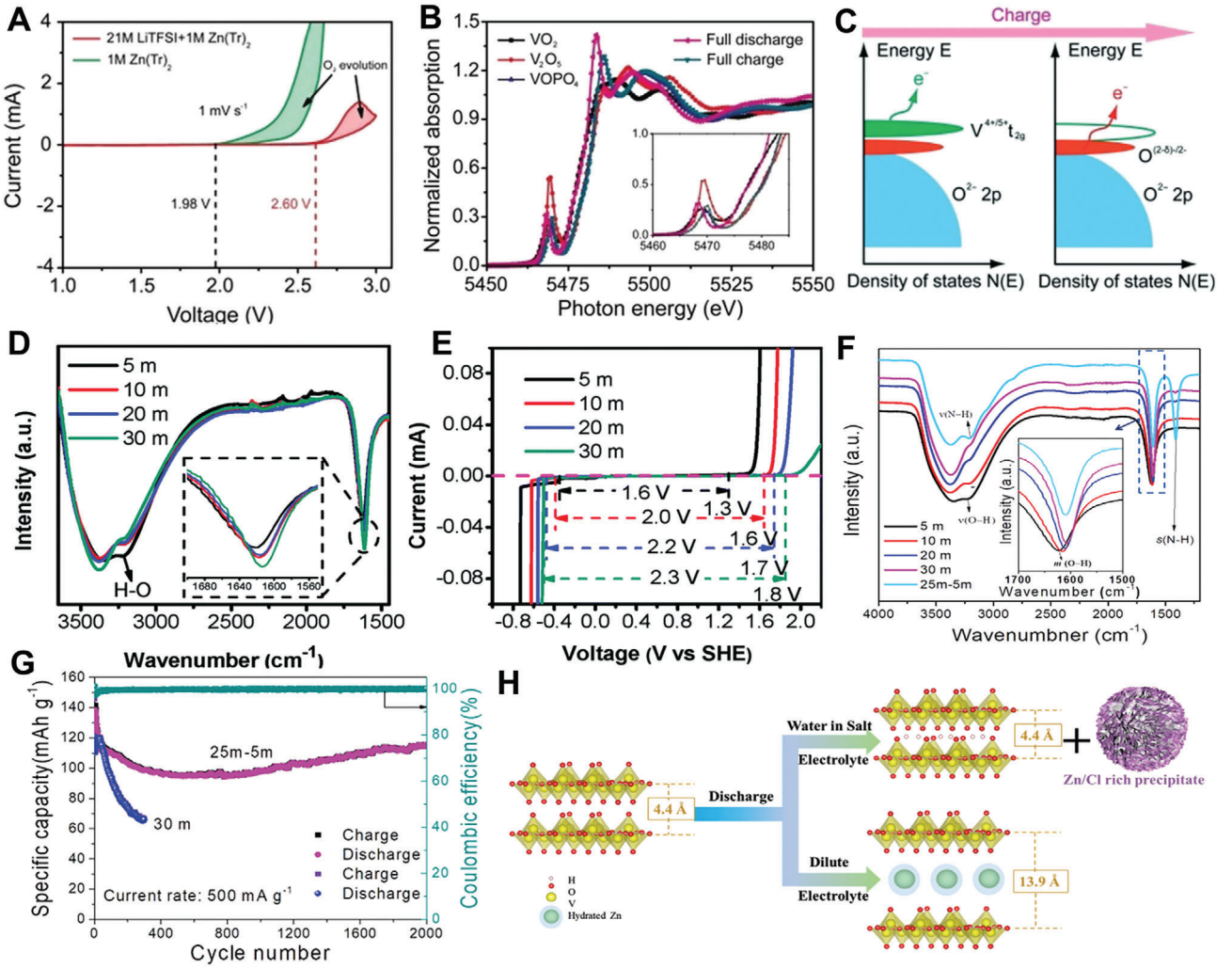

Figure 6. A) CV curves of Zn electrodes in different electrolytes. B) Vanadium K-edge XANES spectra collected for the initial, full discharged, and fully charged states. C) Diagram of energy versus density of states in $VOPO_4$/SWCNT electrodes. Reproduced with permission.[47] Copyright 2019, WILEY-VCH. D) FTIR spectra and E) electrochemical stability window of the $ZnCl_2$ electrolyte at different concentrations. Reproduced with permission.[48] Copyright 2018, The Royal Society of Chemistry. F) FTIR spectra with various salt concentrations. G) The cycle lifespan profiles of the NVPOF electrode in the 25 M + 5 M electrolyte (red) and 30 M electrolyte (blue) at a current rate of 0.5 A g^{-1}. Reproduced with permission.[51] Copyright 2020, Wiley-VCH. H) Schematic illustration of the dynamic structural evolution for V_2O_5 cathode in different concentration electrolytes. Reproduced with permission.[52] Copyright 2021, WILEY-VCH.

3.1. Water-In-Salt Typed High Concentration Electrolytes

Under certain conditions, the ionic conductivity of electrolytes is related to the concentration of electrolyte salts and grows with increasing salt concentration, mainly because the distance between the central Zn^{2+} and the solvents and anions shortens when increasing concentration, intensifying the interfacial interaction.[13c,15a] Previous studies of ZIBs had pointed out that the solvent structure mechanism of metal ions was found to be similar to that of lithium ion battery systems. Indeed, high-concentration salt electrolyte systems can regulate the solvation shell in the electrolyte and effectively improve the electrode/electrolyte interface stability, forming electrolyte salts-derived solid electrolyte interphase, thus extending the cycle life of battery.[45] However, due to the decrease of surrounding temperature, the dissolution of electrolyte salts becomes lower and that is necessary to adjust the salt concentration of the electrolyte to make it suitable for low temperature conditions. However, it should be noted that high-concentration electrolyte may solve multiple problems,[46] which not only slows the dissolution and corrosion of the electrode, but also reduces the freezing point of the electrolyte, expands the voltage window and improves the ion migration number, etc, which seems like the ionic liquid additives in the conventional electrolytes to regulate the inner Helmholtz layer.

Introducing high concentration salt system into vanadium-based ZIBs not only extends the cycle life, but also effectively reduces the dissolution of cathode materials, raising the capacity retention rate. After employing 21 M LiTFSI/1 M $Zn(Tr)_2$ as the electrolyte for Zn//$VOPO_4$ full battery, Niu et al. discovered that the voltage of oxygen evolution reaction in **Figure 6**A was greatly enlarged, and there was no obvious oxygen absorption reaction

© 2023 The Authors. Advanced Energy Materials published by Wiley-VCH GmbH

16146840, 0, Downloaded from https://onlinelibrary.wiley.com/doi/10.1002/aenm.202304010 by Karlsruher Institut F., Wiley Online Library on [15/01/2024]. See the Terms and Conditions (https://onlinelibrary.wiley.com/terms-and-conditions) on Wiley Online Library for rules of use; OA articles are governed by the applicable Creative Commons License

even when charged to 2.1 V, while the redox peaks still appeared in the high-voltage region. The X-ray near-edge structure analysis (XANE) of V in the K-edge (Figure 6B) also illustrated that the redox reaction occurred in the high-voltage region. In the relationship of energy versus density of states in Figure 6C, it is found that an electron will be lost from oxygen to generate a localized electron hole on the oxygen during the first charging from the open-circuit voltage to 2.1 V, since the energy of the oxidation of V^{5+} is below the oxygen valence band. On discharging from 2.1 to 1.7 V, the electron will be returned to oxygen. On further discharging from 1.7 to 0.8 V, the electron will occupy the t_{2g} state of octahedrally coordinated $VOPO_4$, corresponding to a slight increase in interlayer spacing. In contrast, at the fully discharged state, owing to the strong electrostatic attraction between inserted Zn^{2+} ions and oxygen in the layers, the interlayer spacing decreased. These results show that increasing the plateau voltage of the battery to 1.56 V promotes the reversibility of the crystal structure conversion of $VOPO_4$ during charge/discharge, resulting in an excellent rate performance and a long cycle life of up to 1000 cycles with a capacity retention of 93%.[47] As depicted in the Fourier transform infrared (FTIR) analysis of Figure 6D, when the concentration of $ZnCl_2$ increases from 5 to 30 mol L^{-1}, the H-O-H bending vibration red-shifts from 1623 to 1612 cm^{-1}, likely corresponding to the increased viscosity. Meanwhile, in the O-H stretching band, the symmetric stretch (3200 $cm^{-1)}$ decreases and asymmetric stretch (3400 cm^{-1}) increases. It means that the high concentration salt electrolyte can wipe off undesirable side reaction products $Zn(OH)_2$ and ZnO through disturbing the hydrogen bond network binding with Zn^{2+}. Meanwhile, the high concentration salt electrolyte can greatly broaden the electrochemical stability window range (Figure 6E).[48] However, follow-up investigations have identified that the pH value of the electrolyte also has a great impact on the cycle stability. For example, alkaline electrolytes tend to form $Zn(OH)_4^{2-}$ or ZnO on the metallic Zn surface that result in low Coulombic efficiency;[49] while acidic electrolytes would interact with the vanadium-based electrodes, resulting in poor cycle stability and severe capacity decay.[49c,50]

Subsequently, a neutral double-salt aqueous electrolyte composed of 25 M $ZnCl_2$/5 M NH_4Cl was designed by Bai et al.[51] Fourier Transform Infrared Spectrometer (FTIR) displayed that the peak intensity of the -NH group gradually weakened at 3206 cm^{-1} as the $ZnCl_2$ salt concentration increased, and the bending vibration signal of O-H also shifted to the low wavenumber from 1623 to 1606 cm^{-1}. Figure 6F illustrated that there were more electrolyte ions filling between the water molecules, leading to the desolvation effect by breaking the hydrogen bonds as solute molecules compete for ligand environment. Meanwhile, the introduction of NH_4Cl into the electrolyte act as the buffer and regulated the pH value of the electrolyte. Consequently, the capacity decay of $Na_3V_2(PO_4)_2O_{1.6}F_{1.4}$ (NVPOF) cathode was significantly suppressed at 0.5 A g^{-1} and the lifespan lasted up to 2000 cycles (Figure 6G). However, the mechanism of zinc ion storage in high-concentration salt electrolyte remains unknown. An in-depth analysis of reaction mechanism of high-concentration salt and the structural evolution in the absence of water was performed by Ma et al.[52] To gain insight into the dynamic diffusion kinetics of H^+ and Zn^{2+} in V_2O_5, the migration paths were depicted in detail by the aid of theoretical simulation (Figure 6H), which revealed that H^+ possessed a lower diffusion barrier than Zn^{2+} (0.10 vs 6.57 eV) because of the smaller size. The aforementioned results also confirm that in the high-concentration salt system, hydrogen ions are the main contributors to the capacity, while the V_2O_5 cathode in the low-concentration electrolyte will experience severe lattice expansion from 4.4 Å to 13.9 Å (319%) due to the dehydration intercalation of zinc ions, enlarging the layer space distance. That means the application of high-concentration salt system would effectively suppress the lattice expansion and significantly avoid high internal stress and large volumetric changes in the V_2O_5 cathode.

Metal ions have strong electrostatic interactions with dipolar water molecules, and the solidification fundamental reason for the most aqueous electrolytes is that the bonding rate of hydrogen bonds is faster than the breaking rate. In this case, the introduction of concentrated electrolytes can break the hydrogen bonding network and thus inhibit the solidification of water.[2c,15a] Chen's group realized the rupture of the pristine hydrogen bonding network in the $ZnCl_2$-based electrolyte by modulating the solvation shell structure, which can effectively reduce the number of hydrogen bonds in active water molecules and inhibit the solidification of free water, thus significantly lowering the solid-liquid transition temperature (Tt) of the aqueous electrolyte.[2c] When a high-concentration electrolyte contains 1 M $Zn(CF_3SO_3)_2$ and 21 M LiTFSI, the quasi-solid-state battery can operate at -15 °C and achieve a capacity of 60 mAh g^{-1} at a current density of 0.5 A g^{-1}.[53] Although much improvements have been achieved, several challenges in high-concentration salt electrolytes under low-temperature environments remain intractable, such as increased viscosity, decreased conductivity, salting-out at low temperatures, and high cost.[15a] Consequently, the implementation of high-concentration salt electrolytes in zinc-ion batteries still requires some practices to be considered.

3.2. Solvation Shell Reconstruction with Organic Additives

In contrast to high concentration salt electrolyte systems, the hydrophobicity of organic additives is adopted to make it preferentially adsorb at the electrode interface to form localized region of high concentration, thus isolating the active water and electrode and expanding the electrochemical window.[2e,54] Additionally, the solidification point of the optimized electrolyte can be lowered due to the destruction of the hydrogen bonding network in the low temperature environment of the mixed electrolyte,[3a] ensuring a much higher ionic conductivity than that of pure matter. Not only that, the electrolyte additives also change the solvation shell and regulate the coordination environment of zinc ions via crowed strategies, which can slow down the severe solvation phenomenon at low temperature,[15b] thus allowing the battery to express excellent rate performance and cycle capacity at low temperature. The key breakthroughs and electrochemical performances of vanadium base cathodes using organic additives are summarized in Table 1.

In general, the migration of Zn^{2+} is the dominate one in conventional aqueous electrolyte. The Zn^{2+} coordinates with six neighboring water molecules to form a solvated $Zn(H_2O)_6^{2+}$, thus stabilizing the migration in the electrolyte. Unfortunately, the large ionic radius of solvated $Zn(H_2O)_6^{2+}$ makes it extremely challenging to dissociate and transport across the

© 2023 The Authors. Advanced Energy Materials published by Wiley-VCH GmbH

16146840, 0, Downloaded from https://onlinelibrary.wiley.com/doi/10.1002/aenm.202304010 by Karlsruher Institut F., Wiley Online Library on [15/01/2024]. See the Terms and Conditions (https://onlinelibrary.wiley.com/terms-and-conditions) on Wiley Online Library for rules of use; OA articles are governed by the applicable Creative Commons License

Table 1. Organic additives for achieving high-performance LT-VZIBs.

Basic Electrolyte	Organic Additive	Cycling Performance [mAh g^{-1}]	Key Breakthroughs and Discovery	Refs.
2 M $ZnSO_4$	40 vol% ethylene glycol	113 @ 0.2 A g^{-1} for 250 cycles	• Solvation structure regulation ✓ Working temperature: −40°C	[3a]
3 M Zn $(CF_3SO_3)_2$	20 vol% propylene carbonate	183 @ 0.1 A g^{-1} for 300 cycles	• Cathode dissolution suppression ✓ Working temperature: −40°C	[2e]
1 M Zn $(CF_3SO_3)_2$	72 vol% acetonitrile	51.25 @ 2 A g^{-1} for 10000 cycles	• Zn^{2+} kinetics promotion ✓ Working temperature: −40°C	[66]
1 M Zn $(CF_3SO_3)_2$	methanol methanol	160 @2 A g^{-1} (rate performance)	• $Zn(H_2O)_2(CH_3OH)_2^{2+}$ formation ✓ Working temperature: −40°C	[67]
1 M Zn $(CF_3SO_3)_2$	70 vol% tetrahydrofurfuryl alcohol	79.61 @0.06 A g^{-1} for 200 cycles	• Solvation structure regulation ✓ Working temperature: −20°C	[68]
2 M Zn $(CF_3SO_3)_2$	40 vol% trimethyl	50.8 @0.5 A g^{-1} for 12000 cycles	• $Zn^{2+}[H_2O]_{5.02}[TMP]_{0.14}[OTf^-]_{0.84}$ formation ✓ Working temperature: −40°C	[69]
2 M $ZnSO_4$	Phosphate N, N-dimethyl acetamide	152.8 @1 A g^{-1} for 500 cycles	• Hydrogen-bonding network reform ✓ Working temperature: −50°C	[70]
1 M Zn $(CF_3SO_3)_2$	oligomer poly(ethylene glycol) dimethyl	77.8 @0.1 A g^{-1} for 1000 cycles	• Solvation structure regulation ✓ Working temperature: −18°C	[71]
3 M $Zn(CF_3SO_3)_2$ +0.1 M ZnI_2	10 vol% ethylene glycol	83.3 @0.2 A g^{-1} for 200 cycles	• Solvation structure regulation ✓ Working temperature: 0°C	[72]
2 M Zn $(CF_3SO_3)_2$	50 vol% trimethyl phosphate	209.3 @1 A g^{-1} for 1200 cycles	• Cathode dissolution suppression ✓ Working temperature: −20°C	[73]
			✓ Working temperature: 0°C	

electrode/electrolyte interface and insert inside the cathode interior, considerably limiting the potential to participate in internal ion exchange and deteriorating the performance and utilization.[55] Subsequently, the polar propylene carbonate (PC) as an additive is introduced into 3 M $Zn(CF_3SO_3)_2$ electrolyte. The PC-added electrolytes are still colorless and transparent at room temperature with the growing of the ratio of PC in the mixed electrolyte (**Figure** 7A). This may be attributed to the amphipathic structure of zinc trifluoromethanesulfonate ($Zn(OTf)_2$), which acts as the electrolyte and the anionic surfactant at the same time and solve the poor intersolubility between H_2O and PC. The viscosity of the electrolyte gradually increased with the introduction of PC, which contributed to the difficulty of Zn^{2+} diffusion and the decline of ionic conductivity (Figure 7B). This also implies that the PC can change the intrinsic water-dominated solvation shell structure. The FTIR spectra in Figure 7C suggested that the hydrogen bonds (3000-3500 cm^{-1}) between active water molecules were destroyed and the coordination environment of central Zn^{2+} was altered by the addition of PC. Afterwards, the electrolyte coupled with $NaV_3O_8{\cdot}1.5H_2O$ (NVO) cathode for stabilizing 6 days was further characterized by mass spectrometer. The results illustrated that only very low concentrations of elemental V were dissoluted and detected in P0 and P20, indicating that the dissolution of vanadium-based cathode in the electrolyte was substantially attenuated. It explained why the high capacity retention rate of 98.5% was achieved after 200 cycles for the NVO cathode in P20 electrolyte. More importantly, the Zn|P20|NVO battery also exhibit outstanding performance at −40°C. It delivers a high capacity of 183 mAh g^{-1} and maintains a capacity retention of 100% after 300 cycles at 0.1 A g^{-1}, while the capacity of Zn|P0|NVO dramatically decrease to 0 (Figure 7D). In comparison to previously reported aqueous batteries, the Zn|P20|NVO battery also delivers superior electrochemical stability and high reversibility at low-temperature (Figure 7E).[2e] Similarly, to decrease the extra weight of organic additives, researchers embark on the task of looking for small organic molecules, such as polyaspartic acid (PASP), to regulate the deposition behavior of zinc ions without lowering the ionic conductivity. The adsorption of PASP on the zinc metal surface is the key to realize the smooth and compact deposition of Zn. The surface energy of Zn (100) and Zn (001) planes before and after PASP adsorption are compared in Figure 7F,G.[56] The Zn (001) has significantly lower surface energy (51.1 meV $Å^{-2}$) than that of the (100) plane (77.8 meV $Å^{-2}$). Therefore, the metal zinc grows anisotropically during the deposition process. After PASP adsorption, the surface energy is disproportionately reduced and become almost same, e.g. −4.9 meV $Å^{-2}$ and −4.7 meV $Å^{-2}$ for the surface energy of the regulated Zn (001) and (100), respectively (Figure 7F,G). With the practical PASP-containing electrolyte, the formation of by-product $Zn_4SO_4(OH)_6{\cdot}xH_2O$ is inhibited and the corrosion of

© 2023 The Authors. Advanced Energy Materials published by Wiley-VCH GmbH

16146840, 0, Downloaded from https://onlinelibrary.wiley.com/doi/10.1002/aenm.202304010 by Karlsruher Institut F., Wiley Online Library on [15/01/2024]. See the Terms and Conditions (https://onlinelibrary.wiley.com/terms-and-conditions) on Wiley Online Library for rules of use; OA articles are governed by the applicable Creative Commons License

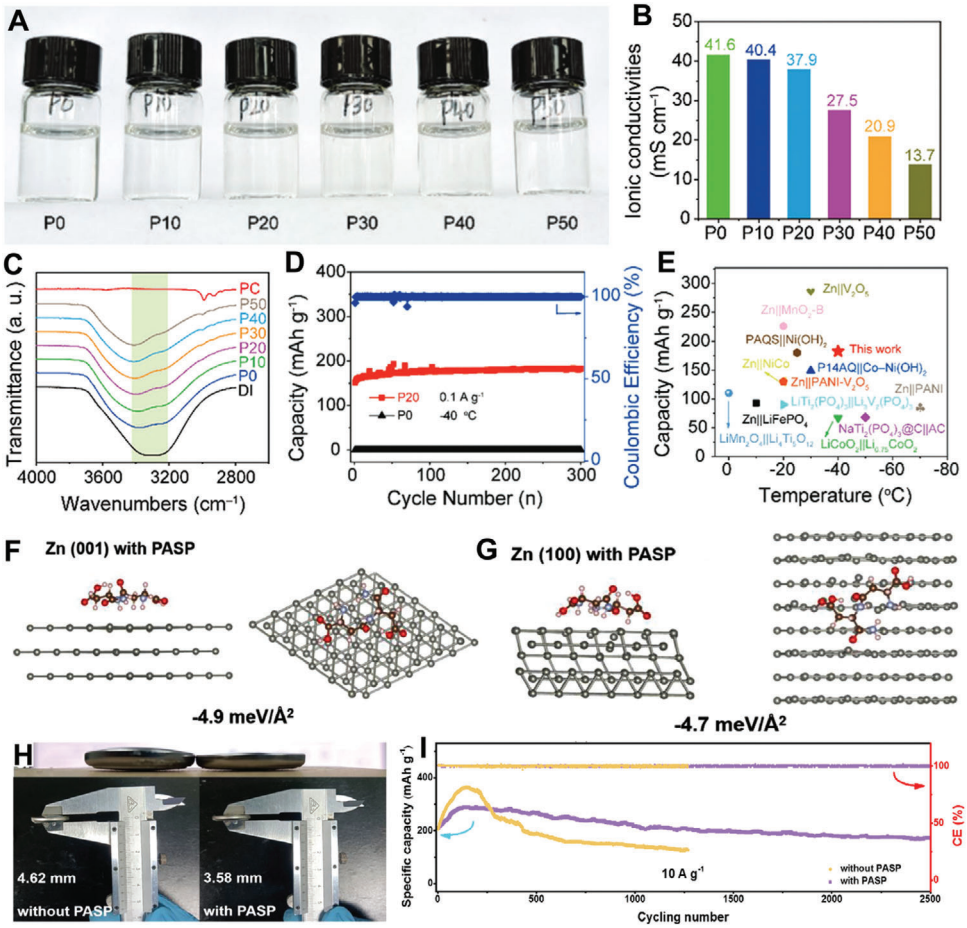

Figure 7. A) The optical photographs of the mixed electrolytes. B) The ionic conductivity of the mixed electrolytes at different compositions. C) Raman spectra vibration signals of O-H in H_2O, PC, and different PC added electrolytes. D) Cycling performance of the Zn|P20|NVO button battery at −40°C. E) Comparison of the capacity at low temperature for Zn|P20|NVO battery and other reported aqueous batteries. Reproduced with permission.[2e] Copyright 2022, WILEY-VCH. F,G) Comparison of the surface energies for the Zn (001) and Zn (100) after PASP adsorption. H) Swelling extent comparison for the coin cells assembled in the electrolyte without/with PASP after 100 cycles. I) Cycling performance at 10 A g^{-1} for the Zn//V_2O_5 full cells assemble using the electrolyte without or with PASP additive. Reproduced with permission.[56] Copyright 2021, Elsevier.

zinc flakes is more difficult than that in bare $ZnSO_4$ electrolyte. At the same time, gas evolution in the coin cell is significantly alleviated during the repeated charge-discharge cycling. The coin cell assembled with PASP-free electrolyte swells severely (thickness 4.62 mm) while that assembled using PASP-containing electrolyte swell a little bit (3.58 mm) after cycling (Figure 7H), thus extending the lifespan of Zn//V_2O_5 full cells with nearly 100% Coulombic efficiency at 10 A g^{-1} after 2500 cycles (Figure 7I).

Obviously, at the initial stage, the influence of organic additives on the interfacial reaction was overlooked. In later studies, it was found that the special functional groups in these organic additives could brebuild and reconstruct the interface between electrolyte and electrode for fast desolvation.[57] Generally speaking, desolvation can be realized by adding organic small molecule electrolytes at room temperature without changing ionic conductivity, greatly inhibiting the side reactions at the interface and achieving durable long cycle life.[56,58] As a typical case, monosodium glutamate (MSG) has caught much attention as a small molecule organic additive thanks to its advantages of low cost and high efficiency. As depicted in **Figure** 8A, the bright metallic zinc surface turned gray when soaked in pristine $ZnSO_4$ electrolyte with unexpected side reactions, while another zinc disk still exhibited a metallic shine surface with no obvious morphological changes or by-products formed on the Zn surface after adding 0.1 M MSG into the pristine electrolyte. As confirmed, the Glu^- anion generated from MSG was preferentially adsorbed on the surface of Zn anode, forming an isolation layer between water molecules and metallic Zn surface to eliminate their direct contact, thus inhibiting the side reactions. Apart from that, the MSG decorated $ZnSO_4$ electrolyte exhibited a stable current density after a shorter 2D diffusion (Figure 8B). Density functional theory (DFT) calculations similarly demonstrated that the Glu- anion was more likely to preferentially bind with Zn^{2+} rather than water molecules, thus promoting the desolvation of hydrated $Zn(H_2O)_6^{2+}$. As illustrated in the schematics (Figure 8C), in pure $ZnSO_4$ electrolyte, Zn^{2+} was deposited uncontrollably on the Zn surface due to water adsorption and solvation phenomena, eventually leading to random zinc dendrites. In contrast, after the introduction of MSG (Figure 8D), a physical barrier adsorbed on the Zn surface was formed by Glu-adsorption,

© 2023 The Authors. Advanced Energy Materials published by Wiley-VCH GmbH

16146840, 0, Downloaded from https://onlinelibrary.wiley.com/doi/10.1002/aenm.202304010 by Karlsruher Institut F., Wiley Online Library on [15/01/2024]. See the Terms and Conditions (https://onlinelibrary.wiley.com/terms-and-conditions) on Wiley Online Library for rules of use; OA articles are governed by the applicable Creative Commons License

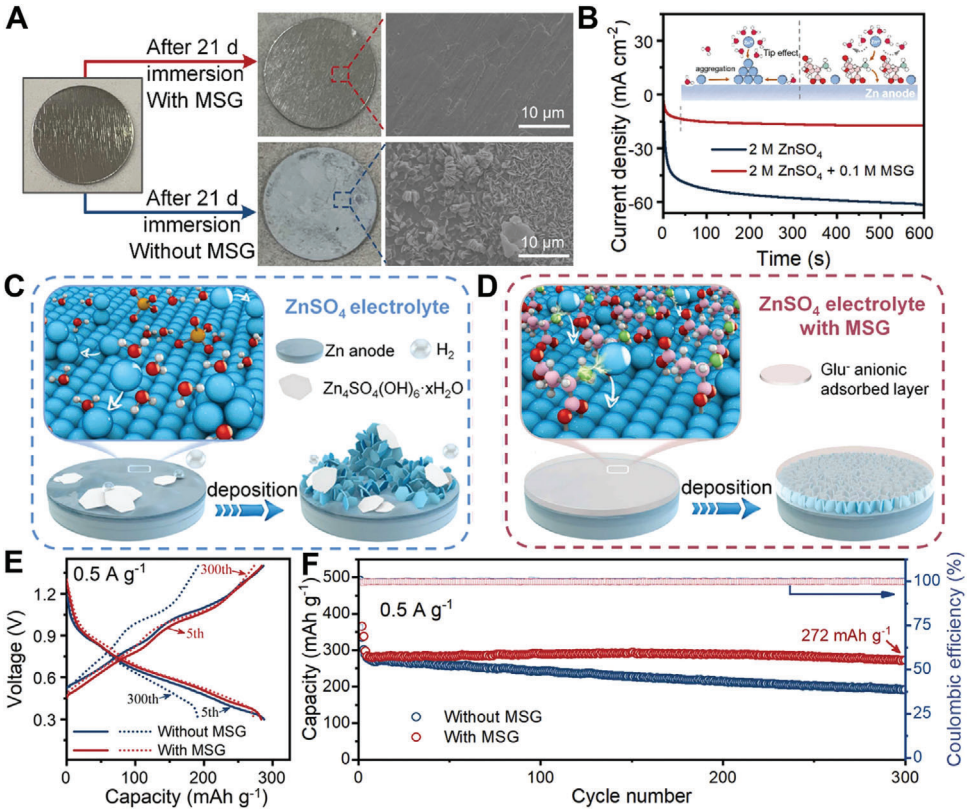

Figure 8. A) Optical images and SEM images of polished Zn before and after 21-day immersion. B) Chronoamperograms of Zn metal in $ZnSO_4$ electrolyte with and without MSG. C) Schematics of zinc dendrite formation and severe hydrogen evolution reaction during Zn deposition in $ZnSO_4$ electrolyte. D) Schematics of the formation of a flat zinc metal-water isolation layer during Zn deposition in $ZnSO_4$ electrolyte with MSG. E) Voltage profiles at different cycles and F) corresponding cycling performance at 0.5 A g^{-1} of $NH_4V_4O_{10}$//Zn cells in $ZnSO_4$ electrolyte with and without MSG. Reproduced with permission.[58] Copyright 2022, Elsevier.

inhibiting the hydrogen evolution reactions. Even more critically, when Zn^{2+} was involved in the electron exchange, the adsorbed Glu^- anion redistributes the zinc ion flux and promotes the interfacial desolvation of hydrated zinc ions, leading to uniform zinc deposition and fast zinc ion transport kinetics. As a result, the assembled $NH_4V_4O_{10}$||Zn cells with MSG electrolyte additive delivered ultra-high capacity retentions of 96% at 0.5 A g^{-1} after 300 cycles and 93.6% at 2 A g^{-1} after 1000 cycles (Figure 8E,F),[58] much better than those without MSG additive (66.6% at 0.5 A g^{-1}, 38.9% at 2 A g^{-1}).

Considering the solvation effect of $Zn(H_2O)_6^{2+}$ and the increased interfacial diffusion resistance caused by the solidification of electrolyte at low temperature,[2e,15a] ethylene glycol (EG) was applied as an electrolyte additive into the $ZnSO_4$ electrolyte to form a hybrid electrolyte with outstanding zinc ion conductivity and superior reversibility. The molecular dynamics simulations (MD simulations) (**Figure 9A**) indicated that the solvation structure of Zn^{2+} in the electrolyte allowed the binding of SO_4^{2-}, EG, and H_2O with the coordination number as well as the diffusion coefficient of Zn^{2+} in different electrolytes as shown in Figure 9B. With the increase of EG content, the diffusion coefficient of Zn^{2+} first increased and then decreased, indicating that the solvation structure of Zn^{2+} ligated with EG and H_2O contributed to the rapid transport of Zn^{2+}. DFT calculations yielded that the relative binding energies of Zn^{2+} to anions or solvent molecules (Zn^{2+}—SO_4^{2-}>Zn^{2+}—EG>Zn^{2+}—H_2O) (Figure 9C), explaining that Zn^{2+} preferentially coordinates with EG compared to H_2O molecules. Besides, the introduction of EG apparently decreased the electrostatic potential of Zn^{2+}–5H_2O at solvated state, which was conducive to the rapid transport of Zn^{2+}-related species (Figure 9D,E). Consequently, the assembled Zn//PANIV_2O_5 battery exhibited excellent rate performance at -20 °C with a specific capacity of 130 mAh g^{-1} under a current density of 0.1 A g^{-1} (Figure 9F).[3a] In addition, the PC additives also afforded the Zn//P20//NVO battery with a charming cycle stability at -40 °C. Despite the co-insertion of H^+ and H_2O caused by dissolution and precipitation during the discharge processes, the introduction of PC additive significantly changed this phenomenon (Figure 9G). A local high-concentration PC location formed between the NVO electrode and electrolyte effectively separated the cathode from active H_2O, thus desirably suppressing the dissolution of NVO and HER formation (Figure 9H). Remarkably, a large solvation shell induced by the excessive P50 concentration may disrupt the NVO lattice and lead to continuous capacity decay (Figure 9I).[2e] The equivalent effect can be obtained at low temperature by adding organic reagents such as PC, [10] EG,[14] NMP,[59] etc. It is also feasible to obtain low concentrations of non-solidifying electrolytes, thereby enabling superior electrochemical performance of LT-VZIBs at low temperatures.

© 2023 The Authors. Advanced Energy Materials published by Wiley-VCH GmbH

16146840, 0, Downloaded from https://onlinelibrary.wiley.com/doi/10.1002/aenm.202304010 by Karlsruher Institut F., Wiley Online Library on [15/01/2024]. See the Terms and Conditions (https://onlinelibrary.wiley.com/terms-and-conditions) on Wiley Online Library for rules of use; OA articles are governed by the applicable Creative Commons License

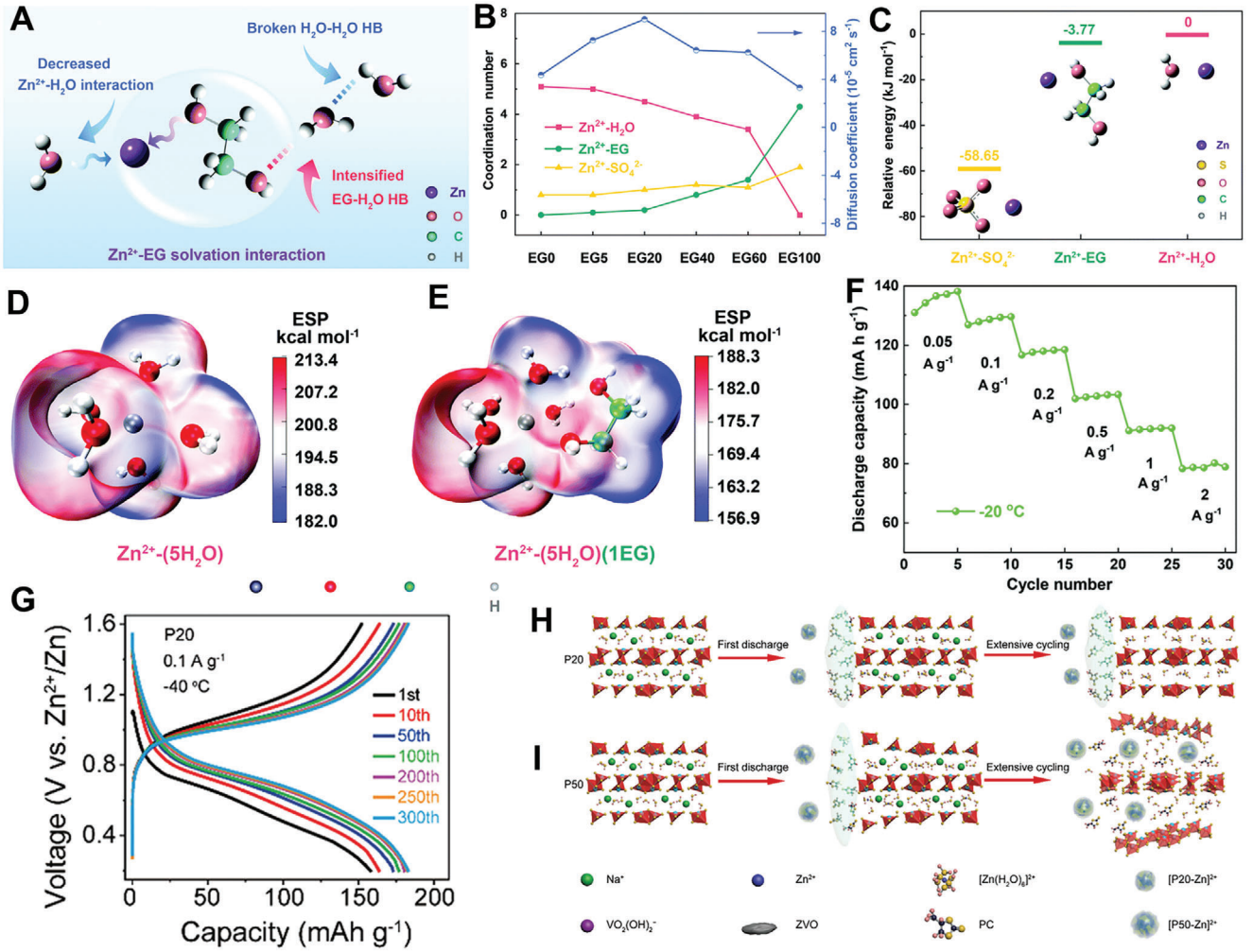

Figure 9. A) Schematic illustration of a possible mechanism of how the Zn^{2+}-EG solvation interaction impacts the chemistry of the hybrid electrolyte. B) Coordination numbers of H_2O, EG, and SO_4^{2-} around Zn^{2+} and diffusion coefficient of Zn^{2+} in different electrolytes calculated from MD simulations. C) Relative binding energy for Zn^{2+} with different species obtained from DFT calculations. D,E) Electrostatic potential maps of the original Zn^{2+}-H_2O system and the added-EG system. F) Rate performance of EG40 at -20 °C with various current densities ranging from 0.05 to 2.0 A g^{-1}. Reproduced with permission.[3a] Copyright 2020, The Royal Society of Chemistry. G) Discharge/charge voltage profiles of the Zn//P20//NVO button battery at -40 °C. H,I) Schematic illustrations of structure evolutions of NVO during continuous Zn^{2+} insertion/extraction processes in P20 and P50 electrolyte, respectively. Reproduced with permission.[2e] Copyright 2022, WILEY.

It is worth noting that the addition of organic electrolyte can in situ generate solid electrolyte interface (SEI) layer, which is usually composed of organic and inorganic ingredients. Generally, the SEI layer possesses outstanding ion sieving behavior and structural flexibility, which can quickly conduct Zn^{2+} as well as effectively mitigate the side reactions about water. Covalent organic frameworks (COFs) have been known as a kind of porous crystalline materials with designable structures and extremely ordered mass transfer channels.[60] Park et al.[61] designed a single Zn^{2+} conducting electrolytes based on a zinc sulfonated covalent organic framework COF (TpPa-$SO_3Zn_{0.5}$) for aqueous zinc-ion batteries. The as-prepared TpPa-$SO_3Zn_{0.5}$ electrolyte displayed structural stability against water through chemically stable β-ketonimine linkages. Because of well-defined directional channels and immobilized sulfonates which are covalently tethered to directional pores, the TpPa-$SO_3Zn_{0.5}$ display outstanding Zn^{2+}-sieving behavior and homogeneous Zn^{2+} flux, exhibiting the conductivity as high as 2.2×10^{-4} S cm^{-1}. In addition, TpPa-$SO_3Zn_{0.5}$ with ionomeric buffer function can effectively prevent the structural disruption of cathode during repeated redox process, ultimately achieving ultrahigh performance aqueous zinc-ion batteries with the plating/stripping lifespan as high as 500 h. Meanwhile, an ultrathin and uniform 3D COOH-functionalized covalent organic frameworks film with high mechanical strength was designed on the surface of Zn anodes.[60] Consequently, the 3D-COOH-COF film can not only selectively accelerate Zn^{2+} ion and inhibiting anions transport for enhancing Zn ion diffusion, but also inhibiting the occurrence of hydrogen evolution reaction (HER) on the electrode surface. In short, COFs show great promise as solid electrolyte or protective layer in aqueouos zinc ion batteries (AZIBs) due to its unique pore structure and adjustable surface chemistry for sieving and averaging the ion flux.

© 2023 The Authors. Advanced Energy Materials published by Wiley-VCH GmbH

16146840, 0, Downloaded from https://onlinelibrary.wiley.com/doi/10.1002/aenm.202304010 by Karlsruher Institut F., Wiley Online Library on [15/01/2024]. See the Terms and Conditions (https://onlinelibrary.wiley.com/terms-and-conditions) on Wiley Online Library for rules of use; OA articles are governed by the applicable Creative Commons License

Indeed, it is challengeable to develop all-weather aqueous Zn based batteries with acceptable performance due to the quite sluggish reaction kinetics under low temperatures. Typically, low temperature AZIBs (LT-AZIBs) often suffer from retarded ion transport and severe solvation behaviors not only in the frozen aqueous electrolyte, but also at/across the cathode/electrolyte interface and inside cathode interior, significantly limiting the practical performance of LT-ZIBs. To further broaden the working temperature for wide application, diethylene glycol monoethyl ether (DG) was introduced by Zhang et al as an electrolyte additive to enhance Zn battery performance within a wide temperature range from −35 to 65°C. The introduction of DG into a non-concentrated aqueous electrolyte of $Zn(OTF)_2$ disrupts the initial hydrogen bonding network of the aqueous electrolyte, reconstructing the solvation structure surrounding Zn^{2+} for fast diffusion kinetics. At the same time, the reductive decomposition of coordinated DG and OTF^- can lead to the formation of a self-healing inorganic/organic ZnF_2-ZnS SEI layer during battery operation, effectively mitigating the detrimental side reactions to realize long cycling duration Zn based batteries under wide temperature range, which is potential to be extended to the all-weather VZIBs in the future.[62]

3.3. Gel Electrolyte

Although the aqueous electrolytes possess high ionic conductivity and low viscosity, they also have inevitable deficiencies. Firstly, the dissolution of the vanadium-based cathode materials in the aqueous electrolyte leads to capacity decay. Secondly, the contact area of the liquid electrolyte cancels out under stress. Last but not least, the solidification of the liquid electrolyte at low temperature leads to a reduction of the contact area with the electrode interface, which greatly hinders the reaction kinetics at the interface.[15a] Nevertheless, gel electrolyte strategy can inhibit the dissolution of active materials, effectively restrain the growth of zinc dendrites, and maintain a high ionic conductivity. Besides, the anti-freezing gel electrolyte also delivers satisfactory capacity at high and low temperatures.

To achieve long-term reversible Zn stripping/plating behaviors, a zwitterionic polymer gel electrolyte has been applied to assemble quasi-solid-state ZIBs, in which the zwitterionic polymer is a type of polymer with charged anionic and cationic groups on the branches or main chain. This gel electrolyte exhibits record-high room temperature ionic conductivity of 32.0 mS cm^{-1} and Zn ions transference number of 0.656.[63] As illustrated in **Figure 10**A, the strong interactions between water molecules and charged groups enabled zwitterionic polymers to exhibit a robust water-retaining capacity. Furthermore, the charged groups promoted a favorable adhesion between the electrolyte and electrode interface, rendering a uniform ion distribution on the electrode surface with a high ion transfer number and uniform ion distribution. As demonstrated in Figure 10B, the as-prepared gel electrolyte could be quickly restored to its original state after 20 twists. The cut ordinary gel and the blue dyed gel still manifested the ability to withstand a weight of 200 g upon placement for 24 h after bonding together through self-healing ability, which also proved its strong self-healing capability and mechanical strength. As a hydrogel with chemical crosslinking, the obtained gel electrolyte offered exquisite mechanical properties with a high-water content above 87% exposed at 50°C for 24 h (Figure 10C). Consequently, it displayed exceptional rate performance and long-cycle stability when coupled with VS_2 cathode.

However, conventional gel electrolytes tend to freeze below zero degree, sacrificing their mechanical properties and ionic conductivity and leading to poor cycling performance. Accordingly, developing gel electrolytes for anti-freeze is essential to ensure high performance and long lifespan LT-VZIBs.[25b,64] A polyacrylamide (PAAm)/dimethyl sulfoxide (DMSO)/$Zn(CF_3SO_3)_2$ multi-component hydrogel electrolyte (PDZ-H) was proposed owing to the unique 3D cross-linked network of PAAm,which displayed a wide working temperature (Figure 10D). Besides, the coordination of the anionic groups on the chain with Zn^{2+} affects the Zn^{2+} distribution and inhibits the growth of zinc dendrites. At the same time, DMSO not only forms a solid electrolyte interphase layer on the electrode surface to increase cycling stability, but also has strong hydrogen bonds toward water to decrease the freezing point. And thus, the ionic conductivity of the PDZ-H electrolyte gradually increases with elevated temperature even in a wide temperature range from −40 to 60 °C. As revealed by the CV curves at a scan rate of 2 mV s^{-1}, the redox peaks of $Zn_3V_2O_8$//Zn/PDZ-H full battery are maintained well in the temperature ranging from −40 to 60 °C. The capacity-voltage curves also disclose that the zinc storage mechanism during charge/ discharge behaves similarly with changed temperature (Figure 10E). Unexpectedly, the full cell stabilized normally for 300 days at a current density of 2 A g^{-1} under -40 °C (Figure 10F).[65]

Owing to the exceptional elasticity of polymer matrices and their fewer water feature, hydrogels are useful for stabilizing electrode reactions and preventing interfacial dislocation. The functional polymers in the gel electrolyte would benefit to confine the activity of the water molecules against the dissolution of active materials and the occurrence of unfavorable side reactions, i.e., HER. When the temperature decreases to below freezing point, the hydrogel electrolyte is deemed to encounter complex interfacial issues like aqueous electrolyte. In this case, the electrolyte/electrode interfacial contact and anti-freezing properties of the current hydrogel electrolytes would be challenging for practical applications in zinc-ion batteries. Nevertheless, rarely report is focused on the development of low temperature hydrogel electrolyte for LT-ZIBs. To make the anti-freeze mechanism of the hydrogel clearer, it is potential to resort to diverse in-situ and ex-situ technologies, such as interfacial sensitive in-situ sum frequency generation (SFG), in-situ Raman, time-of-flight secondary ion mass spectrometer (TOF-SIMS), to detect the evolution of the related interface from the room temperature to the freezing point or to elaborate the interfacial information under the all-weather temperature. In virtue of these in/ex-situ technologies, it is convenient to investigate the interactions among salt ions, water molecules, and hydrophilic polymer chains in depth, understanding the impact of local liquid phase components and domain-limited ion migration chains in hydrogels on the mass transfer processes and electrochemical reaction at the interface. At the same time, the following points must be taken into account: i) constructing a well-adhered hydrogel electrolyte/electrode interface by the synergy of tough hydrogel matrix and chemical interfacial interaction (electrostatic interactions, van der Waals

© 2023 The Authors. Advanced Energy Materials published by Wiley-VCH GmbH

16146840, 0, Downloaded from https://onlinelibrary.wiley.com/doi/10.1002/aenm.202304010 by Karlsruher Institut F., Wiley Online Library on [15/01/2024]. See the Terms and Conditions (https://onlinelibrary.wiley.com/terms-and-conditions) on Wiley Online Library for rules of use; OA articles are governed by the applicable Creative Commons License

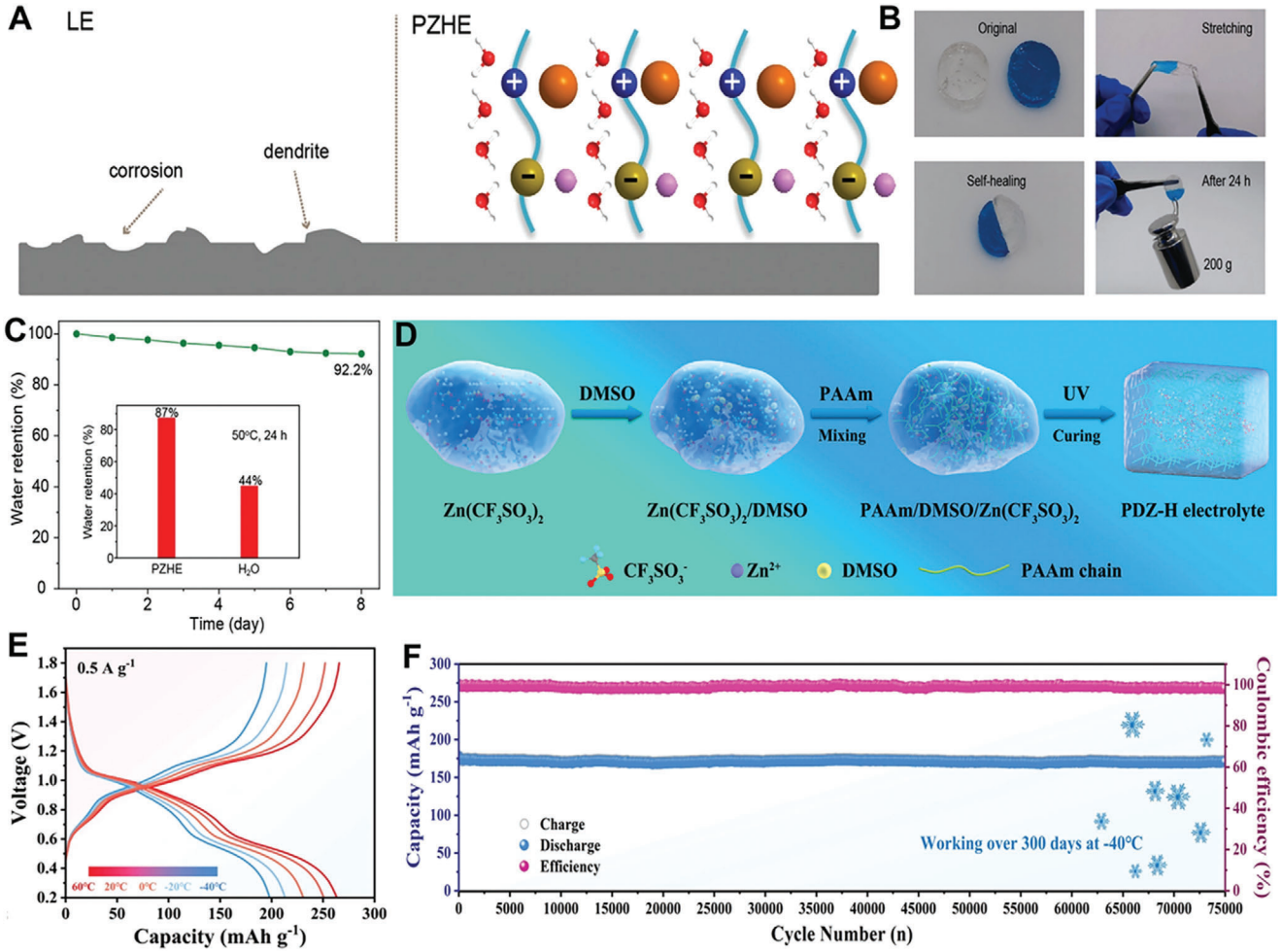

Figure 10. A) Schematic illustration of the morphologies of Zn metal anode with LE/PZHE during Zn plating. B) Self-healing behavior of the hydrogel electrolyte with and without blue colorant. C) Water retention capacity of PZHE. Reproduced with permission.[63] Copyright 2020, WILEY. D) Schematic diagram of synthesis process of the PDZ-H electrolyte. E) Capacity-voltage curves at different temperature from 60 to -40 °C. F) Long-term cyclic stability of the $Zn_3V_2O_8$//Zn//PDZ-H full cell. Reproduced with permission.[65] Copyright 2022, WILEY.

interactions, hydrogen bonds and hydrophobic interactions), enabling fast ion kinetics at the interface; ii) improving anti-freezing ability of hydrogel electrolyte and low-temperature ionic conductivity is crucial to ensure high performance and long lifespan LT-VZIBs.

Above all, in terms of electrolyte optimizations, strategies of high concentration salt electrolyte, organic additive electrolyte and gel electrolyte are summarized. For example, high concentration salts are effective in improving the structural stability of cathode materials and hindering the growth of dendrite, but its application is limited due to the high cost and the decreased salt solubility at low temperature. Organic additives play crucial roles in regulating the solvation structure of zinc ions and inhibiting the uncontrollable growth of dendrites. Organic small molecules are mostly employed to inhibit side reactions and make zinc ions uniformly deposited, while organic reagents are engaged in reducing the desolvation energy barrier and thus greatly improving the low-temperature performance. The gel electrolytes have absolute advantages over liquid electrolytes in terms of widening the operating voltage window and building a stable interface. It is obvious that LT-VZIBs are adequately researched with regard to electrolytes, but the focus for energy density improvement of LT-VZIBs still lies on cathode modification, which has substantial blanks to be supplemented.

4. Summary and Prospect

Vanadium-based compounds feature outstanding theoretical specific capacity, moderate voltage plateau, and wide paths for Zn^{2+} diffusion, providing a critical option for improving the energy densities of ZIBs with long lifespan. Decreasing the working temperature from room to low temperature condition, LT-VZIBs unavoidably face with deteriorated and dissatisfactory electrochemical performances due to the much-depressed dynamics desolvation/diffusion kinetics. In low-temperature operation, the large solvation/desolvation energy barrier of $[Zn(H_2O)_6]^{2+}$ at the electrode/electrolyte interface is too crucial to dissociate for releasing free Zn^{2+}, leading to unsatisfied rate capacity and cycle stability. To this end, the performances of LT-VZIBs are highly dependent on decreasing the desolvation energy barrier at the

© 2023 The Authors. Advanced Energy Materials published by Wiley-VCH GmbH

16146840, 0, Downloaded from https://onlinelibrary.wiley.com/doi/10.1002/aenm.202304010 by Karlsruher Institut F., Wiley Online Library on [15/01/2024]. See the Terms and Conditions (https://onlinelibrary.wiley.com/terms-and-conditions) on Wiley Online Library for rules of use; OA articles are governed by the applicable Creative Commons License

electrode/electrolyte interface and reducing freezing point without sacrificing ion conductivity.

Bearing this in mind, we systematically reviewed the kinetics modulation strategies base on the recent advances in the cathode and electrolyte toward high-performance LT-VZIBs. In detail, the vanadium-based cathode construction strategies in hetero ion doping and enrichment of anion/cation vacancies are summarized, which aims at improving the electron and ionic conductivity or expanding layer spacing to widen pathways for transport of free Zn^{2+}. On the other hand, in order to decrease the freezing point of electrolyte, passivate interfacial water molecules, and reduce the desolvation energy barrier, various electrolyte regulations for reconstructions of solvation shells through high-concentration electrolytes, electrolyte additives and gel electrolytes strategies are summarized. Although the worldwide efforts on the LT-VZIBs, the studies are still at its early stage, especially there lacks a comprehensive and systematic demonstration on the relations of the low temperature performance with the interfacial Zn^{2+}desolvation and diffusion kinetics. The following aspects to further enhance the development of LT-VZIBs should be paid more attentions.

4.1. Developing New Electrochemically-Strengthened Cathode with Highly Adjustable Electron Density for Fast Electron/Ion Kinetics

In the low-temperature operations, the ideal cathode materials should afford rapid electronic conductivity, fast dissociation kinetics from solvated structures to generate bare free Zn^{2+}, and fast ion diffusion kinetics across the interface and in the cathode's interior. As discussed above, metallic cations or non-metallic anions doping, and defect engineering can redistribute the local electronic density to form high electronic conductivity and fast ion diffusion kinetics, and inhibit the structure destroy after insertion/extraction at the same time. Similarly, the desolvation behaves like a chemical reaction, contributing to higher barriers. In the future, one possibly could take advantages of catalysis to reduce the desolvation and diffusion barriers, so that reach the goal of all-weather performance. As well known, catalytic strategy proposed in battery field is greatly associated with the redistribution of the electronic state between the catalyst and reactant. Recently, single atomic catalysts (SACs) are confirmed to be effective in decreasing the interfacial desolvation energy barriers and ion diffusion energy barriers in Li metal-based batteries, due to their unique electronic state induced high activity. Defective vanadium-based compounds have potential to provide affluent anchoring sites and controllable coordination numbers to modulate the coordination environment and the geometric structure of the ligand site on the concentration and activity of SACs. In this regard, future investigations should be devoted to the exploitation of various kinds defective vanadium-based compounds that are affluent in coordination structures and adjustable electron structures, which is beneficial for constructing stable SACs strengthened vanadium-based cathode with strong activity for high-performance LT-VZIBs. Under low temperature, the behaviors of hydrate Zn^{2+} seems to be a disaster and rate-determining step owing to the limited kinetics and huge desolvation barriers. With optimized modification of the cathodes such as defect engineering and SACs implantation, it provides sufficient active site to help to dissociate the large-size hydrate Zn^{2+} and form uniform CEI layer, so that the V-dissolution would be avoided and prevented under the low current density. Therefore, the stability of zinc-vanadium batteries with low current density at low temperature is also of great important for practical application.

4.2. Extracting the Zn Storage Mechanism from Combination of Theoretical Simulations with Ex/In-Situ Characterizations

So far, vanadium-based AZIBs display controversial Zn storage mechanisms under low temperature operations. Generally, the cathodes sometimes face phase transition or metal dissolution with reaction proceeding. At the same time, foreign ions (Zn^{2+}) insertion result in different conditions for the vanadium-based compounds because the de-intercalation of Zn^{2+} induces cathode expansion or even structural collapse. This structural change poses a great uncertainty to the release of capacity and cycle stability of the battery, let alone to find the exact storage mechanism. To further enhance the capacity and cycle stability, the introduction of doping atoms within the cathode' interior may enable higher intrinsic conductivity of vanadium-based compounds to facilitate lower reaction energy barriers, the excess amounts of heteroatom tend to inhibit Zn^{2+} ion insertion by occupying available spaces. Under the extra influence of the icing electrolyte with low temperature, this doping strategy would make the Zn storage mechanism more complicated and confusing. As one solution, catalytic sites can grant easy desolvation of free Zn^{2+} from solvated structures and rapid Zn^{2+} diffusion, but would not hinder the intercalation of Zn^{2+}. Another is using ex/in-situ characterizations such as in-situ XRD, TEM, and XAS on the vanadium-based compounds to exactly trace the structure and morphology evolution with the reaction processing or TOF-SIMS to observe the state of the vanadium-based cathode before and after Zn^{2+} intercalation, so as to establish more precise theoretical simulation for uncovering exact Zn storage mechanism. Based on the obtained exact Zn storage mechanism, the corresponding improvement strategies are adopted to further optimize the electrode and realize a high energy density LT-VZIBs.

4.3. Tracing the Real Time Interfacial Evolution Including Zn^{2+} Desolvation, CEI Formation, and Zn^{2+} Diffusion

Owing to the solidification of electrolyte at low temperature, the interfacial diffusion resistance would significantly be increased with the formation of solvation effect on $Zn(H_2O)_6{}^{2+}$. As a result, severe solvation shell with higher force leads to sluggish Zn ion transport and huge energy barriers at the electrode interface and interior. To lower the interfacial energy barriers for boosting the Zn ion kinetics, the desolvation of $Zn(H_2O)_6{}^{2+}$ structures as well as their chemical interactions with the vanadium-based compounds or their influence on the growth quality of the cathode/electrolyte interphase (CEI) should be reorganized at the premise of understanding the interfacial information from molecules and atomic level. Up to date, little information on interface molecules and their motion states has been available on previous reports. Special operando optical characterizations such

© 2023 The Authors. Advanced Energy Materials published by Wiley-VCH GmbH

16146840, 0, Downloaded from https://onlinelibrary.wiley.com/doi/10.1002/aenm.202304010 by Karlsruher Institut F., Wiley Online Library on [15/01/2024]. See the Terms and Conditions (https://onlinelibrary.wiley.com/terms-and-conditions) on Wiley Online Library for rules of use; OA articles are governed by the applicable Creative Commons License

as in situ sum frequency generation (SFG) and in situ Raman have potential to be introduced into this field to real-time dynamic monitor the state of interface water molecules during solvated Zn^{2+} deintercalation, which is of immense assistance in the design and construction of a new interfacial layer. Tracing the real time interfacial evolution is of great importance to recognize the desolvation process of the $Zn(H_2O)_6^{2+}$ structures to free bare Zn^{2+} and their following diffusion process, which is helpful to evaluate the chemical kinetics at the atomic and molecular levels and diagnose the accurate binding energy of active sites in electrode materials to Zn^{2+}. Such interfacial in-situ characterizations supported theoretical simulations ensure a much clearer elucidate the relationship between structure and performance.

4.4. Screening Suitable Cathode Structure to Fasten Interfacial Desolvation and Diffusion

In conventional aqueous electrolyte, the Zn^{2+} coordinates with six neighboring water molecules to form a solvated $Zn(H_2O)_6^{2+}$, in order to stabilize the migration in the electrolyte. Unfortunately, the large ionic radius of solvated $Zn(H_2O)_6^{2+}$ makes it extremely challenging to dissociate and transport across the electrode/electrolyte interface and insert inside the cathode's interior, especially under the low temperature operation. High performance is only achievable when suitable features like fast interfacial Zn^{2+} desolvation and diffusion allowed by well-designed cathodes. As a result, it is necessary to implement a desired cathode optimization to generate fast interfacial desolvation kinetics for releasing more Zn^{2+} and accelerating the free Zn^{2+} diffusion into the cathode's interior to realize rapid reactions. Based on the large number of optimization strategies, theoretical simulation is a beneficial tool to significantly simplify the experimental steps to screen out the most suitable cathode with well-arranged interface depending on the important parameters of Zn^{2+} desolvation and diffusion energy barriers. At the same time, saving the experimental cost a lot.

4.5. Synthesizing Compatible All-Weather Electrolytes with LT-VZIBs System for Fast Electrochemical Kinetics

As we all know that the chemical properties of electrolyte determine freezing point, interface electrochemistry, solvation shell structure at extreme low temperature conditions. Generally, the electrochemical activity of the vanadium-based cathodes in the aqueous electrolytes is strongly dependent on surrounding temperature due to their higher freezing point. With the decrease of the temperature to below 0 °C, the solidification of solvent would increase the viscosity with cross-linked hydrogen bond to cause sharp decrease of ionic conductivity, introduce huge energy barriers at the same time to hinder the interfacial Zn^{2+} desolvation, Zn^{2+} diffusion at both the interface, the interior of the cathode. The current strategies in high-concentration salt electrolytes, organic additive electrolytes, hydrogel electrolytes enable VZIBs realizing desired performance at room temperature, however, the large voltage hysteresis, long-time instability are still waiting for being addressed at low temperature. As research proceeded, the ideal low temperature electrolyte should be endowed the features of high desolvation, fast ion transport kinetics, low temperature electrochemical stability, wide working voltage window, low voltage hysteresis, not merely requiring the decrease of freezing point. On the other hand, highly compatible all-weather electrolytes have also potential to guide the Zn^{2+} desolvation, diffusion, deposition in a uniform manner through diverse regulation mechanism for accelerating ion diffusion, greatly extending the service life of the LT-VZIBs at the premise of effectively expanding the working temperature ranges from -40 to 60 °C. The mechanism of electrode-hydrogel electrolyte interaction is still a complex, underexplored issue, which is necessary to be focused to reveal the intricacies of the electrode/electrolyte interface in the future researches relying on divers in-situ, ex-situ technologies, such as interfacial sensitive in-situ SFG, in-situ Raman, TOF-SIMS. Similar to the aqueous electrolyte, an efficient approach to suppress the water freezing within the hydrogel is the adoption of additives, how to choose, modulate additive concentrations to balance the ionic conductivity, anti-freezing ability at the premise of keeping excellent mechanical stability should be further thought. Therefore, it is urgent to screen more electrolytes to match well with the LT-VZIBs to remedy the remained problems in current electrolytes. By the way, the suspended electrolyte with catalytic functions in the Li metal battery field has already been reported to stabilize the migration in the electrolyte, ensure the fast interfacial desolvation, free metal ion transport, through regulation the solvation structure, interfacial construction simultaneously. In this regard, perhaps, the electrolyte with catalytic suspending addictive to enable high-entropy electrolyte is the most promising one, compatible with both the cathode, anode similar Li electrolyte.

Acknowledgements

L.J., H.H., and X.C. contributed equally to this work. The authors acknowledge the National Key R&D Program of China (2021YFA1201503), National Natural Science Foundation of China (No. 21972164, 22279161;12264038, 22309144), the Natural Science Foundation of Jiangsu Province (BK. 20210130), Innovative and Entrepreneurial Doctor in Jiangsu Province (JSSCBS20211428), China Postdoctoral Science Foundation (No. 2023M732561, 2023M731084), Shanghai Sailing Program of China (23YF1408900), Scientific Research Programm-Shaanxi Provincial Education Department (20JS104). J.W. acknowledge the funding provided by the Alexander von Humboldt Foundation and the basic funding of the Helmholtz Association. Dr. Y. Z. Zhang thanks the Shanghai Super Postdoctoral Incentive Program. The authors also thank the support from Nano-X, Suzhou Institute of Nano-tech and Nano-bionics, Chinese Academy of Sciences

Open access funding enabled and organized by Projekt DEAL.

Conflict of interest

The authors declare no conflict of interest.

Keywords

aqueous zinc ion batteries, desolvation behaviors, interface engineering, low temperature, vanadium-based cathodes

Received: November 23, 2023
Revised: December 18, 2023
Published online:

© 2023 The Authors. Advanced Energy Materials published by Wiley-VCH GmbH

16146840, 0, Downloaded from https://onlinelibrary.wiley.com/doi/10.1002/aenm.202304010 by Karlsruher Institut F., Wiley Online Library on [15/01/2024]. See the Terms and Conditions (https://onlinelibrary.wiley.com/terms-and-conditions) on Wiley Online Library for rules of use; OA articles are governed by the applicable Creative Commons License

[1] a) Y. Shang, D. Kundu, *Joule* **2023**, *7*, 244; b) R. F. Service, *Science* **2021**, *372*, 890; c) Y. Liang, Y. Yao, *Nat. Rev. Mater.* **2022**, *8*, 109; d) L. E. Blanc, D. Kundu, L. F. Nazar, *Joule* **2020**, *4*, 771; e) Z. Zhu, T. Jiang, M. Ali, Y. Meng, Y. Jin, Y. Cui, W. Chen, *Chem. Rev.* **2022**, *122*, 16610; f) X. Zhang, X. Li, Y. Zhang, X. Li, Q. Guan, J. Wang, Z. Zhuang, Q. Zhuang, X. Cheng, H. Liu, J. Zhang, C. Shen, H. Lin, Y. Wang, L. Zhan, L. Ling, *Adv. Funct. Mater.* **2023**, *33*, 2302624; g) J. Zhang, R. He, L. Jia, C. You, Y. Zhang, M. Liu, N. Tian, H. Lin, J. Wang, *Adv. Funct. Mater.* **2023**, *33*, 2305674; h) P. Chen, T. Wang, D. He, T. Shi, M. Chen, K. Fang, H. Lin, J. Wang, C. Wang, H. Pang, *Angew. Chem. Int. Ed. Engl.* **2023**, *62*, e202311693; i) Y. Lyu, J. A. Yuwono, P. Wang, Y. Wang, F. Yang, S. Liu, S. Zhang, B. Wang, K. Davey, J. Mao, Z. Guo, *Angew. Chem., Int. Ed.* **2023**, *62*, e202303011.

[2] a) T. He, Y. Ye, H. Li, S. Weng, Q. Zhang, M. Li, T. Liu, J. Cheng, X. Wang, J. Lu, B. Wang, *Mater. Today* **2021**, *43*, 53; b) M. Liao, J. Wang, L. Ye, H. Sun, Y. Wen, C. Wang, X. Sun, B. Wang, H. Peng, *Angew Chem. Int. Ed. Engl.* **2020**, *59*, 2273; c) Q. Zhang, Y. Ma, Y. Lu, L. Li, F. Wan, K. Zhang, J. Chen, *Nat. Commun.* **2020**, *11*, 4463; d) H. Geng, M. Cheng, B. Wang, Y. Yang, Y. Zhang, C. C. Li, *Adv. Funct. Mater.* **2019**, *30*, 1907684; e) D.-S. Liu, Y. Zhang, S. Liu, L. Wei, S. You, D. Chen, M. Ye, Y. Yang, X. Rui, Y. Qin, C. C. Li, *Adv. Funct. Mater.* **2022**, *32*, 2111714; f) H. Li, Z. Chen, L. Zheng, J. Wang, H. Adenusi, S. Passerini, H. Zhang, *Small Methods* **2023**, e2300554; g) G. Li, L. Sun, S. Zhang, C. Zhang, H. Jin, K. Davey, G. Liang, S. Liu, J. Mao, Z. Guo, *Adv. Funct. Mater.* **2023**, 2301291.

[3] a) N. Chang, T. Li, R. Li, S. Wang, Y. Yin, H. Zhang, X. Li, *Energ. Environ. Sci.* **2020**, *13*, 3527; b) J. Wang, J. Zhang, J. Wu, M. Huang, L. Jia, L. Li, Y. Zhang, H. Hu, F. Liu, Q. Guan, M. Liu, H. Adenusi, H. Lin, S. Passerini, *Adv. Mater.* **2023**, *35*, 2302828; c) H. Tu, L. Li, Z. Wang, J. Wang, H. Lin, M. Wang, C. Yan, M. Liu, *ACS Nano* **2022**, *16*, 16898; d) J. Wang, J. Zhang, S. Duan, L. Jia, Q. Xiao, H. Liu, H. Hu, S. Cheng, Z. Zhang, L. Li, W. Duan, Y. Zhang, H. Lin, *Nano Lett.* **2022**, *22*, 8008.

[4] a) Z. Qi, T. Xiong, T. Chen, W. Shi, M. Zhang, Z. W. J. Ang, H. Fan, H. Xiao, W. S. V. Lee, J. Xue, *J. Alloys and Compd* **2021**, *870*, 159403; b) Y. Yang, Y. Tang, G. Fang, L. Shan, J. Guo, W. Zhang, C. Wang, L. Wang, J. Zhou, S. Liang, *Energ. Environ. Sci.* **2018**, *11*, 3157; c) K. Zhu, S. Wei, H. Shou, F. Shen, S. Chen, P. Zhang, C. Wang, Y. Cao, X. Guo, M. Luo, H. Zhang, B. Ye, X. Wu, L. He, L. Song, *Nat. Commun.* **2021**, *12*, 6878; d) W. Tang, B. Lan, C. Tang, Q. An, L. Chen, W. Zhang, C. Zuo, S. Dong, P. Luo, *ACS Sustainable Chem. Eng.* **2020**, *8*, 3681.

[5] a) S. Gao, B. Li, H. Tan, F. Xia, O. Dahunsi, W. Xu, Y. Liu, R. Wang, Y. Cheng, *Adv. Mater.* **2022**, *34*, 2201510; b) S. Islam, M. H. Alfaruqi, D. Y. Putro, S. Park, S. Kim, S. Lee, M. S. Ahmed, V. Mathew, Y.-K. Sun, J.-Y. Hwang, J. Kim, *Adv. Sci. (Weinh)* **2021**, *8*, 2002636.

[6] Y. Zeng, J. Xu, Y. Wang, S. Li, D. Luan, X. W. (.D.). Lou, *Angew Chem. Int. Ed. Engl.* **2022**, *61*, 202212031.

[7] a) Z. Liu, Y. Huang, Y. Huang, Q. Yang, X. Li, Z. Huang, C. Zhi, *Chem. Soc. Rev.* **2020**, *49*, 643; b) X. Wang, Y. Li, P. Das, S. Zheng, F. Zhou, Z.-S. Wu, *Energy Storage Mater.* **2020**, *31*, 156; c) D. Zhao, X. Wang, W. Zhang, Y. Zhang, Y. Lei, X. Huang, Q. Zhu, J. Liu, *Adv. Funct. Mater.* **2023**, *33*, 2211412; d) T. Lv, G. Zhu, S. Dong, Q. Kong, Y. Peng, S. Jiang, G. Zhang, Z. Yang, S. Yang, X. Dong, H. Pang, Y. Zhang, *Angew Chem. Int. Ed. Engl.* **2023**, *62*, 202216089.

[8] F. Wan, Z. Niu, *Angew Chem. Int. Ed.* **2019**, *58*, 16358.

[9] H. Chen, J. Huang, S. Tian, L. Liu, T. Qin, L. Song, Y. Liu, Y. Zhang, X. Wu, S. Lei, S. Peng, *Adv. Sci. (Weinh)* **2021**, *8*, 2004924.

[10] a) J. Wang, L. Li, H. Hu, H. Hu, Q. Guan, M. Huang, L. Jia, H. Adenusi, K. V. Tian, J. Zhang, S. Passerini, H. Lin, *ACS Nano* **2022**, *16*, 17729; b) K. Xu, *J. Power Sources* **2023**, *559*, 232652; c) D. Kundu, S. Hosseini Vajargah, L. Wan, B. Adams, D. Prendergast, L. F. Nazar, *Energ. Environ. Sci.* **2018**, *11*, 881.

[11] Y. Shi, Y. Chen, L. Shi, K. Wang, B. Wang, L. Li, Y. Ma, Y. Li, Z. Sun, W. Ali, S. Ding, *Small* **2020**, *16*, 2000730.

[12] a) S. Guo, L. Qin, C. Hu, L. Li, Z. Luo, G. Fang, S. Liang, *Adv. Energy Mater.* **2022**, *12*, 22007302; b) Z. Wang, M. Zhou, L. Qin, M. Chen, Z. Chen, S. Guo, L. Wang, G. Fang, S. Liang, *eScience* **2022**, *2*, 209.

[13] a) X. Wang, B. Xi, X. Ma, Z. Feng, Y. Jia, J. Feng, Y. Qian, S. Xiong, *Nano Lett.* **2020**, *20*, 2899; b) Z. Xing, G. Xu, X. Xie, M. Chen, B. Lu, J. Zhou, S. Liang, *Nano Energy* **2021**, *90*, 106621; c) Y. Zhu, J. Yin, X. Zheng, A.-H. Emwas, Y. Lei, O. F. Mohammed, Y. Cui, H. N. Alshareef, *Energ. Environ. Sci.* **2021**, *14*, 4463; d) H. Y. Asl, A. Manthiram, *Science* **2020**, *369*, 140.

[14] a) J. Cao, D. Zhang, X. Zhang, Z. Zeng, J. Qin, Y. Huang, *Energ. Environ. Sci.* **2022**, *15*, 499; b) J. Hao, B. Li, X. Li, X. Zeng, S. Zhang, F. Yang, S. Liu, D. Li, C. Wu, Z. Guo, *Adv. Mater.* **2020**, *32*, 2003021; c) Q. Kang, Z. Zhuang, Y. Li, Y. Zuo, J. Wang, Y. Liu, C. Shi, J. Chen, H. Li, P. Jiang, X. Huang, *Nano Res.* **2023**, *16*, 9240.

[15] a) Y. Zhao, Z. Chen, F. Mo, D. Wang, Y. Guo, Z. Liu, X. Li, Q. Li, G. Liang, C. Zhi, *Adv. Sci. (Weinh)* **2020**, *8*, 2002590; b) Q. Ma, R. Gao, Y. Liu, H. Dou, Y. Zheng, T. Or, L. Yang, Q. Li, Q. Cu, R. Feng, Z. Zhang, Y. Nie, B. Ren, D. Luo, X. Wang, A. Yu, Z. Chen, *Adv. Mater.* **2022**, *34*, 2207344; c) Q. Zhang, K. Xia, Y. Ma, Y. Lu, L. Li, J. Liang, S. Chou, J. Chen, *ACS Energy Lett.* **2021**, *6*, 2704.

[16] Y. Zhang, Z. Cao, S. Liu, Z. Du, Y. Cui, J. Gu, Y. Shi, B. Li, S. Yang, *Adv. Energy Mater.* **2022**, *12*, 2103979.

[17] M. Chen, S. Xie, X. Zhao, W. Zhou, Y. Li, J. Zhang, Z. Chen, D. Chao, *Energy Storage Mater.* **2022**, *51*, 683.

[18] a) M. Zhao, J. Rong, F. Huo, Y. Lv, B. Yue, Y. Xiao, Y. Chen, G. Hou, J. Qiu, S. Chen, *Adv. Mater.* **2022**, *34*, 2203153; b) R. Meng, H. Li, Z. Lu, C. Zhang, Z. Wang, Y. Liu, W. Wang, G. Ling, F. Kang, Q.-H. Yang, *Adv. Mater.* **2022**, *34*, 2200677; c) Z. Zhang, W. Xu, J. Wang, M. Hu, D. Zhang, L. Jia, A. Kang, Y. Xi, X. Ye, S. Cheng, E. Sun, Y. Chen, Z. Wang, H. Lin, Q. Xiao, *ACS Energy Lett.* **2023**, *8*, 2276.

[19] a) J. Holoubek, H. Liu, Z. Wu, Y. Yin, X. Xing, G. Cai, S. Yu, H. Zhou, T. A. Pascal, Z. Chen, P. Liu, *Nat. Energy* **2021**, *2021*, 303; b) C. B. Jin, N. Yao, Y. Xiao, J. Xie, Z. Li, X. Chen, B. Q. Li, X. Q. Zhang, J. Q. Huang, Q. Zhang, *Adv. Mater.* **2023**, *35*, 2208340; c) X. Zheng, Z. Gu, J. Fu, H. Wang, X. Ye, L. Huang, X. Liu, X. Wu, W. Luo, Y. Huang, *Energ. Environ. Sci.* **2021**, *14*, 4936.

[20] a) Z. Liu, X. Luo, L. Qin, G. Fang, S. Liang, *Adv. Powder Mater.* **2022**, *1*, 100011; b) M. Han, T. C. Li, X. Chen, H. Y. Yang, *Small* **2023**, *8*, 2304901; c) S. Liu, R. Zhang, J. Mao, Y. Zhao, Q. Cai, Z. Guo, *Sci. Adv.* **2022**, *8*, eabn5097.

[21] a) J. Wang, L. Jia, J. Zhong, Q. Xiao, C. Wang, K. Zang, H. Liu, H. Zheng, J. Luo, J. Yang, H. Fan, W. Duan, Y. Wu, H. Lin, Y. Zhang, *Energy Storage Mater.* **2019**, *18*, 246; b) J. Wang, L. Jia, S. Duan, H. Liu, Q. Xiao, T. Li, H. Fan, K. Feng, J. Yang, Q. Wang, M. Liu, J. Zhong, W. Duan, H. Lin, Y. Zhang, *Energy Storage Mater.* **2020**, *28*, 375; c) J. Wang, L. Jia, H. Lin, Y. Zhang, *ChemSusChem* **2020**, *13*, 3404; d) J. Wang, J. Yang, Q. Xiao, J. Zhang, T. Li, L. Jia, Z. Wang, S. Cheng, L. Li, M. Liu, H. Liu, H. Lin, Y. Zhang, *Adv. Funct. Mater.* **2020**, *31*, 2007434; e) J. Wang, S. Cheng, L. Li, L. Jia, J. Wu, X. Li, Q. Guan, H. Hu, J. Zhang, H. Lin, *Chem. Eng. J.* **2022**, *446*, 137291; f) J. Wang, H. Hu, J. Zhang, L. Li, L. Jia, Q. Guan, H. Hu, H. Liu, Y. Jia, Q. Zhuang, S. Cheng, M. Huang, H. Lin, *Energy Storage Mater.* **2022**, *52*, 210; g) J. Wang, H. Hu, S. Duan, Q. Xiao, J. Zhang, H. Liu, Q. Kang, L. Jia, J. Yang, W. Xu, H. Fei, S. Cheng, L. Li, M. Liu, H. Lin, Y. Zhang, *Adv. Funct. Mater.* **2021**, *32*, 2110468; h) Y. Hu, L. Li, H. Tu, X. Yi, J. Wang, J. Xu, W. Gong, H. Lin, X. Wu, M. Liu, *Adv. Funct. Mater.* **2022**, *32*, 2203336; i) L. Li, H. Tu, J. Wang, M. Wang, W. Li, X. Li, F. Ye, Q. Guan, F. Zhu, Y. Zhang, Y. Hu, C. Yan, H. Lin, M. Liu, *Adv. Funct. Mater.* **2023**, *33*, 2212499.

[22] a) Y. Zhang, L. Tao, C. Xie, D. Wang, Y. Zou, R. Chen, Y. Wang, C. Jia, S. Wang, *Adv. Mater.* **2020**, *32*, 1905923; b) J. Wang, S. Cheng, W. Li, S. Zhang, H. Li, Z. Zheng, F. Li, L. Shi, H. Lin, Y. Zhang, *J. Power Sources* **2016**, *321*, 193; c) J. Wang, S. Cheng, W. Li, L. Jia, Q. Xiao, Y. Hou, Z. Zheng, H. Li, S. Zhang, L. Zhou, M. Liu, H. Lin, Y. Zhang,

© 2023 The Authors. Advanced Energy Materials published by Wiley-VCH GmbH

16146840, 0, Downloaded from https://onlinelibrary.wiley.com/doi/10.1002/aenm.202304010 by Karlsruher Institut F., Wiley Online Library on [15/01/2024]. See the Terms and Conditions (https://onlinelibrary.wiley.com/terms-and-conditions) on Wiley Online Library for rules of use; OA articles are governed by the applicable Creative Commons License

Nano Energy **2017**, *40*, 390; d) Z. Liu, L. Qin, X. Cao, J. Zhou, A. Pan, G. Fang, S. Wang, S. Liang, *Prog. Mater. Sci.* **2022**, *125*, 100911; e) J. Ding, H. Zheng, H. Gao, Q. Liu, Z. Hu, L. Han, S. Wang, S. Wu, S. Fang, S. Chou, *Adv. Energy Mater.* **2021**, *11*, 2100973.

[23] a) S. Cheng, J. Wang, S. Duan, J. Zhang, Q. Wang, Y. Zhang, L. Li, H. Liu, Q. Xiao, H. Lin, *Chem. Eng. J.* **2021**, *417*, 128172; b) J. Wang, L. Jia, H. Liu, C. Wang, J. Zhong, Q. Xiao, J. Yang, S. Duan, K. Feng, N. Liu, W. Duan, H. Lin, Y. Zhang, *ACS Appl. Mater. Interfaces* **2020**, *12*, 12727; c) J. Zhang, R. He, Q. Zhuang, X. Ma, C. You, Q. Hao, L. Li, S. Cheng, L. Lei, B. Deng, X. Li, H. Lin, J. Wang, *Adv. Sci. (Weinh)* **2022**, *9*, 2202244; d) S. Cheng, J. Wang, S. Duan, J. Zhang, Q. Wang, Y. Zhang, L. Li, H. Liu, Q. Xiao, H. Lin, *Chem. Eng. J.* **2021**, *417*, 128172.

[24] C. Guo, S. Yi, R. Si, B. Xi, X. An, J. Liu, J. Li, S. Xiong, *Adv. Energy Mater.* **2022**, *12*, 2202039.

[25] a) G. Su, S. Chen, H. Dong, Y. Cheng, Q. Liu, H. Wei, E. H. Ang, H. Geng, C. C. Li, *Nanoscale* **2021**, *13*, 2399; b) W. Zhou, J. Chen, M. Chen, A. Wang, A. Huang, X. Xu, J. Xu, C.-P. Wong, *J. Mater. Chem. A* **2020**, *8*, 8397; c) Y. Yang, Y. Tang, S. Liang, Z. Wu, G. Fang, X. Cao, C. Wang, T. Lin, A. Pan, J. Zhou, *Nano Energy* **2019**, *61*, 617.

[26] Z. Liu, H. Sun, L. Qin, X. Cao, J. Zhou, A. Pan, G. Fang, S. Liang, *ChemNanoMat* **2020**, *6*, 1553.

[27] C. Liu, M. Tian, M. Wang, J. Zheng, S. Wang, M. Yan, Z. Wang, Z. Yin, J. Yang, G. Cao, *J. Mater. Chem. A* **2020**, *8*, 7713.

[28] S. Wu, X. Li, Y. Zhang, Q. Guan, J. Wang, C. Shen, H. Lin, J. Wang, Y. Wang, L. Zhan, L. Ling, *Nano Res.* **2023**, *16*, 9158.

[29] C. Liu, Z. Neale, J. Zheng, X. Jia, J. Huang, M. Yan, M. Tian, M. Wang, J. Yang, G. Cao, *Energ. Environ. Sci.* **2019**, *12*, 2273.

[30] a) F. Zhan, S. Liu, Q. He, X. Zhao, H. Wang, M. Han, Y. Yamauchi, L. Chen, *Energy Storage Mater.* **2022**, *52*, 685; b) Y. Zhao, P. Zhang, J. Liang, X. Xia, L. Ren, L. Song, W. Liu, X. Sun, *Energy Storage Mater.* **2022**, *47*, 424; c) J. Guo, L. Li, J. Luo, W. Gong, R. Pan, B. He, S. Xu, M. Liu, Y. Wang, B. Zhang, C. Wang, L. Wei, Q. Zhang, Q. Li, *Adv. Energy Mater.* **2022**, *12*, 2201481; d) Q. Zang, X. Cheng, S. Chen, Z. Xiao, K.-P. Wang, L. Zong, Q. Zhang, L. Wang, *Chem. Eng. J.* **2023**, *452*, 139396.

[31] H. Chen, Z. Luo, Z. Yang, *J. Electroanalytical Chem.* **2022**, *927*, 116997.

[32] a) J. Zhang, S. Duan, C. You, J. Wang, H. Liu, S. Guo, W. Zhang, R. Yang, *J. Mater. Chem. A* **2020**, *8*, 22240; b) Y. Xi, X. Ye, S. Duan, T. Li, J. Zhang, L. Jia, J. Yang, J. Wang, H. Liu, Q. Xiao, *J. Mater. Chem. A* **2020**, *8*, 14769; c) J. Zhang, C. You, J. Wang, H. Xu, C. Zhu, S. Guo, W. Zhang, R. Yang, Y. Xu, *Chem. Eng. J.* **2019**, *368*, 340.

[33] Z. Ma, K. Rui, Y. Zhang, D. Li, Q. Wang, Q. Zhang, M. Du, J. Yan, C. Zhang, X. Huang, J. Zhu, W. Huang, *Small* **2019**, *15*, 1970116.

[34] a) J. Zhang, L. Jia, H. Lin, J. Wang, *Adv. Energy Sustainability Res.* **2022**, *3*, 2100187; b) J. Zhang, C. You, H. Lin, J. Wang, *Energy Environ. Mater.* **2022**, *5*, 731; c) J. Wang, J. Yang, Q. Xiao, L. Jia, H. Lin, Y. Zhang, *ACS Appl. Mater. Interfaces* **2019**, *11*, 30500.

[35] a) Y. Gao, Z. Liu, S. Guo, X. Cao, G. Fang, J. Zhou, S. Liang, *Energy Environ. Mater.* **2021**, *5*, 186; b) J. Wang, J. Zhang, S. Duan, T. Li, L. Jia, H. Liu, L. Li, S. Cheng, H. Hu, M. Huang, H. Hu, S. Zhang, Q. Xiao, H. Lin, *Chem. Eng. J.* **2022**, *429*, 132352.

[36] a) G. Li, G. R. Blake, T. T. M. Palstra, *Chem. Soc. Rev.* **2017**, *46*, 1693; b) N. Zhang, X. Chen, M. Yu, Z. Niu, F. Cheng, J. Chen, *Chem. Soc. Rev.* **2020**, *49*, 4203.

[37] a) J. Wang, L. Li, H. Hu, H. Hu, Q. Guan, M. Huang, L. Jia, H. Adenusi, K. V. Tian, J. Zhang, S. Passerini, H. Lin, *ACS Nano* **2022**, *16*, 177290; b) J. Wang, J. Zhang, S. Cheng, J. Yang, Y. Xi, X. Hou, Q. Xiao, H. Lin, *Nano Lett.* **2021**, *21*, 3245; c) F. Liu, Q. Yu, J. Xue, B. Shu, C. Zheng, H. Deng, X. Zhang, P. Gong, M. Chen, H. Lin, J. Wang, S. Zhu, J. Wu, *J. Phys. Chem. Lett.* **2022**, *13*, 9501.

[38] D. Zu, H. Wang, S. Lin, G. Ou, H. Wei, S. Sun, H. Wu, *Nano Res.* **2019**, *12*, 2150.

[39] a) M. Du, Z. Miao, H. Li, Y. Sang, H. Liu, S. Wang, *J. Mater. Chem. A* **2021**, *9*, 19245; b) T. He, S. Weng, Y. Ye, J. Cheng, X. Wang, X. Wang, B. Wang, *Energy Storage Mater.* **2021**, *38*, 389; c) X. Li, Q. Guan, Z. Zhuang, Y. Zhang, Y. Lin, J. Wang, C. Shen, H. Lin, Y. Wang, L. Zhan, L. Ling, *ACS Nano* **2023**, *17*, 1653.

[40] J. Krzystek, A. Ozarowski, J. Telser, D. C. Crans, *Coordin. Chem. Rev.* **2015**, *301–302*, 123.

[41] W. Yang, X. Du, J. Zhao, Z. Chen, J. Li, J. Xie, Y. Zhang, Z. Cui, Q. Kong, Z. Zhao, C. Wang, Q. Zhang, G. Cui, *Joule* **2020**, *4*, 1557.

[42] a) L. Ma, S. Chen, N. Li, Z. Liu, Z. Tang, J. A. Zapien, S. Chen, J. Fan, C. Zhi, *Adv. Mater.* **2020**, *32*, 1908121; b) G. Li, Z. Zhao, S. Zhang, L. Sun, M. Li, J. A. Yuwono, J. Mao, J. Hao, J. Vongsvivut, L. Xing, C.-X. Zhao, Z. Guo, *Nat. Commun.* **2023**, *14*, 6526.

[43] L. Ma, M. A. Schroeder, O. Borodin, T. P. Pollard, M. S. Ding, C. Wang, K. Xu, *Nat. Energy* **2020**, *5*, 743.

[44] a) S. D. Pu, B. Hu, Z. Li, Y. Yuan, C. Gong, Z. Ning, C. Chau, S. Yang, S. Zhang, L. Pi, Y. T. Tang, J. Yue, T. J. Marrow, X. Gao, P. G. Bruce, A. W. Robertson, *Joule* **2023**, *7*, 366; b) C. Li, A. Shyamsunder, A. G. Hoane, D. M. Long, C. Y. Kwok, P. G. Kotula, K. R. Zavadil, A. A. Gewirth, L. F. Nazar, *Joule* **2022**, *6*, 1103; c) M. Zhao, Y. Lv, S. Zhao, Y. Xiao, J. Niu, Q. Yang, J. Qiu, F. Wang, S. Chen, *Adv. Mater.* **2022**, *34*, 2206239.

[45] J. Hao, L. Yuan, Y. Zhu, M. Jaroniec, S.-Z. Qiao, *Adv. Mater.* **2022**, *34*, 2206963.

[46] Y. Yamada, J. Wang, S. Ko, E. Watanabe, A. Yamada, *Nat. Energy* **2019**, *4*, 269.

[47] F. Wan, Y. Zhang, L. Zhang, D. Liu, C. Wang, L. Song, Z. Niu, J. Chen, *Angew Chem. Int. Ed. Engl.* **2019**, *58*, 7062.

[48] C. Zhang, J. Holoubek, X. Wu, A. Daniyar, L. Zhu, C. Chen, D. P. Leonard, I. A. Rodríguez-Pérez, J.-X. Jiang, C. Fang, X. Ji, *Chem. Commun.* **2018**, *54*, 14097.

[49] a) W. Wu, X. Yang, K. Wang, Z. Lin, H.-Y. Shi, X. Sun, *Adv. Funct. Mater.* **2022**, *32*, 2207397; b) W. Shang, W. Yu, Y. Liu, R. Li, Y. Dai, C. Cheng, P. Tan, M. Ni, *Energy Storage Mater.* **2020**, *31*, 44; c) X. Zhao, X. Zhang, N. Dong, M. Yan, F. Zhang, K. Mochizuki, H. Pan, *Small* **2022**, *18*, 2200742.

[50] Q. Jian, Y. Wan, J. Sun, M. Wu, T. Zhao, *J. Mater. Chem. A* **2020**, *8*, 20175.

[51] Q. Ni, H. Jiang, S. Sandstrom, Y. Bai, H. Ren, X. Wu, Q. Guo, D. Yu, C. Wu, X. Ji, *Adv. Funct. Mater.* **2020**, *30*, 2003511.

[52] X. Tang, P. Wang, M. Bai, Z. Wang, H. Wang, M. Zhang, Y. Ma, *Adv. Sci. (Weinh)* **2021**, *8*, 2102053.

[53] X. Li, L. Ma, Y. Zhao, Q. Yang, D. Wang, Z. Huang, G. Liang, F. Mo, Z. Liu, C. Zhi, *Mater. Today Energy* **2019**, *14*, 100361.

[54] a) P. Xiong, S. Zhang, R. Wang, L. Zhang, Q. Ma, X. Ren, Y. Gao, Z. Wang, Z. Guo, C. Zhang, *Energ. Environ. Sci.* **2023**, *16*, 3181; b) L. Zhang, R. Wang, Z. Liu, J. Wan, S. Zhang, S. Wang, K. Hua, X. Liu, X. Zhou, X. Luo, X. Zhang, M. Cao, H. Kang, C. Zhang, Z. Guo, *Adv. Mater.* **2023**, *35*, 2210082.

[55] H. Chen, J. Huang, S. Tian, L. Liu, T. Qin, L. Song, Y. Liu, Y. Zhang, X. Wu, S. Lei, S. Peng, *Adv. Sci. (Weinh)* **2021**, *8*, 2004924.

[56] T. Zhou, Y. Mu, L. Chen, D. Li, W. Liu, C. Yang, S. Zhang, Q. Wang, P. Jiang, G. Ge, H. Zhou, *Energy Storage Mater.* **2022**, *45*, 777.

[57] C. Huang, X. Zhao, Y. Hao, Y. Yang, Y. Qian, G. Chang, Y. Zhang, Q. Tang, A. Hu, X. Chen, *Energ. Environ. Sci.* **2023**, *16*, 1721.

[58] Y. Zhong, Z. Cheng, H. Zhang, J. Li, D. Liu, Y. Liao, J. Meng, Y. Shen, Y. Huang, *Nano Energy* **2022**, *98*, 107220.

[59] T. C. Li, Y. Lim, X. L. Li, S. Luo, C. Lin, D. Fang, S. Xia, Y. Wang, H. Y. Yang, *Adv. Energy Mater.* **2022**, *12*, 2103231.

[60] K. Wu, X. Shi, F. Yu, H. Liu, Y. Zhang, M. Wu, H.-K. Liu, S.-X. Dou, Y. Wang, C. Wu, *Energy Storage Mater.* **2022**, *51*, 391.

[61] S. Park, I. Kristanto, G. Y. Jung, D. B. Ahn, K. Jeong, S. K. Kwak, S.-Y. Lee, *Chem. Sci.* **2020**, *11*, 11692.

[62] R. Wang, Q. Ma, L. Zhang, Z. Liu, J. Wan, J. Mao, H. Li, S. Zhang, J. Hao, L. Zhang, C. Zhang, *Adv. Energy Mater.* **2023**, *13*, 2302543.

[63] K. Leng, G. Li, J. Guo, X. Zhang, A. Wang, X. Liu, J. Luo, *Adv. Funct. Mater.* **2020**, *30*, 2001317.

© 2023 The Authors. Advanced Energy Materials published by Wiley-VCH GmbH

16146840, 0, Downloaded from https://onlinelibrary.wiley.com/doi/10.1002/aenm.202304010 by Karlsruher Institut F., Wiley Online Library on [15/01/2024]. See the Terms and Conditions (https://onlinelibrary.wiley.com/terms-and-conditions) on Wiley Online Library for rules of use; OA articles are governed by the applicable Creative Commons License

[64] T. Xu, K. Liu, N. Sheng, M. Zhang, W. Liu, H. Liu, L. Dai, X. Zhang, C. Si, H. Du, K. Zhang, *Energy Storage Mater.* **2022**, *48*, 244.
[65] H. Lu, J. Hu, L. Wang, J. Li, X. Ma, Z. Zhu, H. Li, Y. Zhao, Y. Li, J. Zhao, B. Xu, *Adv. Funct. Mater.* **2022**, *32*, 2112540.
[66] J. Wang, Q. Zhu, F. Li, J. Chen, H. Yuan, Y. Li, P. Hu, M. S. Kurbanov, H. Wang, *Chem. Eng. J.* **2022**, *433*, 134589.
[67] W. Xu, J. Li, X. Liao, L. Zhang, X. Zhang, C. Liu, K. Amine, K. Zhao, J. Lu, *J. Am. Chem. Soc.* **2023**, *145*, 22456.
[68] Y. Qiu, X. Zheng, R. Zhang, Q. Lin, M. Li, J. Luo, S. Yang, Z. Liu, Q. Wang, Y. Yu, C. Yang, *Adv. Funct. Mater.* **2023**, 2023 10825.
[69] W. Wang, S. Chen, X. Liao, R. Huang, F. Wang, J. Chen, Y. Wang, F. Wang, H. Wang, *Nat. Commun.* **2023**, *14*, 5443.
[70] W. Deng, Z. Xu, X. Wang, *Energy Storage Mater.* **2022**, *52*, 52.
[71] Z. Hou, Z. Lu, Q. Chen, B. Zhang, *Energy Storage Mater.* **2021**, *42*, 517.
[72] Y. Yang, S. Guo, Y. Pan, B. Lu, S. Liang, J. Zhou, *Energ. Environ. Sci.* **2023**, *16*, 2358.
[73] B. Qiu, L. Xie, G. Zhang, K. Cheng, Z. Lin, W. Liu, C. He, P. Zhang, H. Mi, *Chem. Eng. J.* **2022**, *449*, 137843.

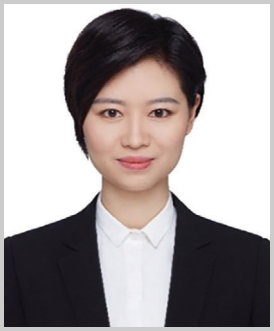

Lujie Jia obtained her Ph.D. degree in Physics from Tsinghua University. She is currently working on the application of new-type battery systems. Her research interest includes the design and synthesis of novel electrode materials, interfacial modification, and the mechanism study of those optimization methods on batteries.

Yongzheng Zhang received his Ph.D. degree from East China University of Science and Technology (ECUST) in 2019. Since 2019, he works as a postdoctoral researcher at Beihang University and ECUST under the supervisions of Prof. Shubin Yang and Prof. Licheng Ling, respectively. His current research interests mainly focus on the 2D electrocatalysts for aqueous zinc-ion batteries and lithium-sulfur batteries.

Jing Zhang is now a assistant researcher in School of Materials Science and Engineering at Xi'an University of Technology, Xi'an, China. She received her Ph.D. degree in Materials Physics and Chemistry at Xi'an University of Technology in 2020. Her researches currently focus on functional catalysis materials synthesis and interface characterization in Li-S batteries.

© 2023 The Authors. Advanced Energy Materials published by Wiley-VCH GmbH

16146840, 0, Downloaded from https://onlinelibrary.wiley.com/doi/10.1002/aenm.202304010 by Karlsruher Institut F., Wiley Online Library on [15/01/2024]. See the Terms and Conditions (https://onlinelibrary.wiley.com/terms-and-conditions) on Wiley Online Library for rules of use; OA articles are governed by the applicable Creative Commons License

Hongzhen Lin is a senior researcher at *i*-lab of Suzhou Institute of Nano-Tech and Nano-bionics, Chinese Academy of Sciences, and University of Science and Technology of China. He majors in developing high energy density lithium metal-based energy storage systems with catalytic functionalities and their in-situ interfacial nonlinear spectroscopy characterization.

Jian Wang is currently a research fellow supported by Alexander von Humboldt foundation in Helmholtz Institute Ulm (HIU) and Karlsruhe Institute of Technology (KIT) after receiving his Ph.D. degree from University of Science and Technology of China. His research interests focus on the applications of catalysis in secondary batteries ("Catalysis-in-Batteries") and the exploration of in-situ characterizations for probing catalytic mechanisms.

© 2023 The Authors. Advanced Energy Materials published by Wiley-VCH GmbH

16146840, 0, Downloaded from https://onlinelibrary.wiley.com/doi/10.1002/aenm.202304010 by Karlsruher Institut F. , Wiley Online Library on [15/01/2024]. See the Terms and Conditions (https://onlinelibrary.wiley.com/terms-and-conditions) on Wiley Online Library for rules of use; OA articles are governed by the applicable Creative Commons License